Stony Brook University

Structural and Electrochemical Studies of High Voltage $Na(Ni_{2/3}Sb_{1/3})O_2$ Cathodes for Secondary Na-ion Batteries

A Thesis Presented

by

Jeffrey Ma

to

The Graduate School

in Partial Fulfillment of the

Requirements

for the Degree of

Master of Science

in

Chemistry

Stony Brook University

May 2014

Stony Brook University

The Graduate School

Jeffrey Ma

We, the thesis committee for the above candidate for the

Master of Science degree, hereby recommend

acceptance of this thesis.

Peter Khalifah – Thesis Advisor
Assistant Professor Department of Chemistry

Kenneth J. Takeuchi – Chairperson of Defense
Professor Department of Chemistry

Michael G. White – Third Member
Professor Department of Chemistry

This thesis is accepted by the Graduate School

Charles Taber
Dean of the Graduate School

Abstract of the Thesis

Structural and Electrochemical Studies of High Voltage $Na(Ni_{2/3}Sb_{1/3})O_2$ Cathodes for Secondary Na-ion Batteries

by

Jeffrey Ma

Master of Science

in

Chemistry

Stony Brook University

2014

Lithium ion batteries have been dominating the energy field in energy storage with its efficiency and performance unmatched. However, the over-exhaustion of the limited amounts of lithium has been causing rising prices. In order to alleviate the use of lithium batteries, scientists have turned some focus to other energy storage alternatives, like sodium batteries. Sodium is abundant, affordable, and environmentally friendly. Sodium batteries have gravimetric energy density comparable to lithium batteries, and are promising for large scale energy grid storage.

In this work, $Na(Ni_{2/3}Sb_{1/3})O_2$ have been synthesized and identified as a sodium battery cathode candidate. An ordered and disordered phase of this layered material has been identified, depending on the temperature used for synthesis. Both phases have been studied structurally using synchrotron radiation and laboratory x-rays. The disordered $Na(Ni_{2/3}Sb_{1/3})O_2$ belongs to the $R\bar{3}m$ space group with the lattice parameters a = 3.0619(6) Å and c = 16.0549(5) Å. The ordered $Na(Ni_{2/3}Sb_{1/3})O_2$ belongs to the C2/m space group with the lattice parameters

a = 5.3048(5) Å, *b* = 9.1847(7) Å , *c* = 5.6285(4) Å. *Ex situ* studies were also performed to study the structural morphology during $Na(Ni_{2/3}Sb_{1/3})O_2$'s electrochemical cycling. The cycling of the material shows a transformation from an initial O3 layered phase to a P3 layered phase during charge, which is reversed during discharge. The electrochemical performance of $Na(Ni_{2/3}Sb_{1/3})O_2$ shows promising results, with the ordered phase being able to yield 133mAh/g capacity.

Acknowledgement

I would like to thank my advisor, Peter Khalifah, for giving me an opportunity to discover this interest in solid state chemistry and battery research. His guidance throughout this journey, and the immense amount of help he gave me during the last few weeks, really means a lot to me.

I would also like to thank my group mates, Alexandra Reinert, Diane Colabello, Andrew Malingowski, Shouhang Bo, Xiaoya Wang, Huafeng Huang, Jue Liu, Michael Saccromanno, Shujie Hu, and Postdoc Dr. Yuri Janssen. They have been very supportive of me throughout this experience, and have helped me countless times throughout the lab. Out of the group, I would like to specifically thank Shouhang Bo again, for being my mentor within the group. I came into the group knowing little to nothing about battery materials and electrochemistry, and Shouhang took on the challenge to teach me everything he knows about the field.

Lastly, I would like to thank my family and friends. Their constant support and words of encouragement fuel me to pursue my dreams and to continue to strive for better.

Table of Contents

1. INTRODUCTION 1

1.1 *Principles of electrochemical storage* 2

1.2 *Lithium ion batteries* 3

1.3 *Sodium ion batteries* 5

1.4 *α-$NaFeO_2$ structure type* 6

1.4.1 *α-$NaFeO_2$ structure* 6

1.4.2 *Lithium Cobalt Oxide ($LiCoO_2$)* 8

1.4.3 *Lithium Nickel Oxide ($LiNiO_2$)* 10

1.4.4 *$A(M_xB_{1-x})O_2$ materials (A=Li, Na; M=Fe, Co, Ni, Cu, Zn; B=Sb, Te, Bi)* 10

2. EXPERIMENTAL 18

2.1 *Preparation of cathode material* 18

2.1.1 *Synthesis of disordered $Na(Ni_{2/3}Sb_{1/3})O_2$* 18

2.1.2 *Synthesis of ordered $Na(Ni_{2/3}Sb_{1/3})O_2$* 19

2.2 *Preparation of electrode and cell construction for electrochemical studies* 22

2.2.1 *Preparation of composite electrode films* 22

2.2.2 *Assembly of battery cells* 22

2.3 *Structural characterization* 23

2.4 *Testing of the electrochemical activity* 24

3. RESULTS AND DISCUSSION 27

3.1 *Structural characterization* 27

3.2 *Electrochemical characterization* 32

3.3 *Ex-situ* x-ray diffraction 43

3.4 *GITT analysis* 47

4. CONCLUSION 50

List of Figures

Figure 1. Basic figure portraying the process within a rechargeable battery. 3
Figure 2. The general overview of the major sodium batteries. This graph also includes well known lithium batteries in blue. 6
Figure 3. Crystal structure of α -$NaFeO_2$. 7
Figure 4. Calculated diffraction pattern of $LiCoO_2$ from Pearson's Crystal Data software. 9
Figure 5. Electrochemical performance of $Li(Ni_{2/3}Sb_{1/3})O_2$ between 2.5 V and 4.6 V at C/20 rate. Reprinted by permission from Elsevier B.V.: X. Ma, K. Kang, G. Ceder, Y.S. Meng, J. Power Sources, 2007, 173, 550-555. Copyright 2007. 12
Figure 6. Electrochemical performance of $Na_2Ni_2TeO_6$ a) charge and discharge between 2.5 V and 4.5 V at 0.03 C and 0.05 C b) charge and discharge between 3.0 V and 4.35 V at 0.03 C. Reprinted by permission from Elsevier B.V.: A. Gupta, C. B. Mullins, and J.B. Goodenough, J. Power Sources, 2013, 243, 817. Copyright 2013. 13
Figure 7. Electrochemical performance of Li_4NiTeO_6 a) showing voltage vs composition b) capacity vs cycle revealing the capacity retention of 100 cycles c) *In-situ x-ray study d) patterns of pristine, charged, and discharged Li_4NiTeO_6 from c).* Reprinted by permission from Royal Society of Chemistry: M. Sathiya, K. Ramesha, G. Rousse, D. Foix, D. Gonbeau, K. Guruprakash, A. S. Prakash, M. L. Doublet, and J.M. Tarascon, Chem. Commun., 2013,49, 11376-11378. Copyright 2013. 14
Figure 8. A light green powder sample of disordered $Na(Ni_{2/3}Sb_{1/3})O_2$ 18
Figure 9. Synthesis process of disordered $Na(Ni_{2/3}Sb_{1/3})O_2$ including pictures of instruments used. 19
Figure 10. The olive-green ordered $Na(Ni_{2/3}Sb_{1/3})O_2$ powder. 20
Figure 11. Synthesis process of ordered $Na(Ni_{2/3}Sb_{1/3})O_2$ including pictures of instruments used. 21
Figure 12 Basic model of a typical battery cell. 23
Figure 13. Disordered $Na(Ni_{2.3}Sb_{1.3})O_2$ cycled between 2.5 V and 4.5 V. Note the significant capacity fading after the first cycle. 25
Figure 14. X-ray diffraction pattern and *R-3m* Rietveld refinement of disordered $Na(Ni_{2/3}Sb_{1/3})O_2$ synthesized at 1000˚C. 28
Figure 15. SEM images of disordered $Na(Ni_{2/3}Sb_{1/3})O_2$ at 1200x magnification (top) and 15000x magnification (bottom). 29
Figure 16. Comparison of XRD patterns of ordered and disordered $Na(Ni_{2/3}Sb_{1/3})O_2$. The ordered phase has sharp superstructure peaks while the disordered phase has broad peaks superstructure which can only be seen for 00l type reflections. 30
Figure 17. X-ray diffraction pattern and C2/m refinement of ordered $Na(Ni_{2/3}Sb_{1/3})O_2$ synthesized at 1200˚C. 31
Figure 18. Comparison of hand ground and ball milled samples of disordered $Na(Ni_{2/3}Sb_{1/3})O_2$. 32
Figure 19. Electrochemical performance of disordered $Na(Ni_{2/3}Sb_{1/3})O_2$ when cycled between 2.5 V and 4.0 V at the rate of C/50 showing its capacity performance (top) and dQ/dV (bottom). 34
Figure 20. Capacity retention of the disordered $Na(Ni_{2/3}Sb_{1/3})O_2$ cell cycled at different C-rates. 36
Figure 21. The first cycle, including charge and discharge, of disordered $Na(Ni_{2/3}Sb_{1/3})O_2$ at different C-rates. 37
Figure 22. Electrochemical performance of disordered $Na(Ni_{2/3}Sb_{1/3})O_2$ cycled with a lower cutoff voltage, from 2.5 V to 3.4 V, at a rate of C/50. 38

Figure 23. Electrochemical performance of ordered $Na(Ni_{2/3}Sb_{1/3})O_2$ when cycled between 2.5 V and 4.0 V at the rate of C/50 showing its capacity performance (top) and dQ/dV (bottom). 40
Figure 24. Capacity retention of the ordered $Na(Ni_{2/3}Sb_{1/3})O_2$ cell cycled at different C-rates. 41
Figure 25: Electrochemical performance of ordered $Na(Ni_{2/3}Sb_{1/3})O_2$ cycled with a lower cutoff voltage, from 2.5 V to 3.4 V, at a rate of C/50. 42
Figure 26. *Ex-situ* studies of disordered $Na(Ni_{2/3}Sb_{1/3})O_2$ showing the X-ray diffraction patterns at different states of charge (top), as well as the electrochemical response of a typical cell (bottom), where * marks peaks from desodiated R3m phase. 44
Figure 27. *Ex-situ* studies of ordered $Na(Ni_{2/3}Sb_{1/3})O_2$ showing the x-ray diffraction patterns at different states of cycling (top) and at which points these different states were stopped during the electrochemical cycling (bottom). Note that top left shows the diffraction patterns in the range of 0˚ to 30˚ 2θ, while the top right shows the range of 4˚ to 5˚ 2θ. 46
Figure 28. GITT of disordered $Na(Ni_{2/3}Sb_{1/3})O_2$ at a rate of C/20 cycled from 2.5 V to 4.0 V. 48
Figure 29. GITT of ordered $Na(Ni_{2/3}Sb_{1/3})O_2$ at a rate of C/50 cycled from 2.5 V to 4.0 V. 49

1. INTRODUCTION

Humanity, as a whole, is also facing a challenge with the consistently growing world population. It is believed that the world population will increase from the current seven billion population, to an estimation of about ten billion by 2050. Current projections for the 2050 population show that energy consumption may increase by three-fold compared to present usage. Countries around the world are growing increasingly more reliant on the consumption of fossil fuels as a source of energy. Due to their limited supply and a growing need to provide energy to an increasing global population, their prices continue to climb. Every year, global energy consumption increases by 2.3%. In order to relieve both the increasing output of pollution and the reliability on non-renewable resources, and to combat the increasing prices for energy, there is a growing demand for the exploration into increasing the usage of renewable energy.

The use of renewable energy dates back to the 1950's and before. However, renewable energy did not become "popularized" until the 1990's, when research in wind and solar energy research began to boom. Electricity is the typical type of energy produced from renewable sources, including wind, solar, hydropower, photovoltaic, biomass, and geothermal means.

Ongoing research on renewable energy has greatly increased the efficiency of these techniques. This has contributed to an increase of renewable energy usage from 3% in the 1950s, and 6% in the 1990s, to 9% in the last three years.[1] The increasing efficiency of renewable energy inevitably leads to a growing demand for the development of better electrical energy storage due to the large variability in power output from many of these sources (wind, solar, etc.). Secondary (or rechargeable) batteries cannot currently meet this critical need for load leveling, but may become suitable for these purposes with further development.

Traditionally, pumped-storage hydroelectricity is used for electrical storage. However, this method is limited by the necessity of certain geographic locations and its high cost to remain operational. Battery materials are more ideal for energy storage as they are not limited by geography. Batteries are normally closed systems where redox reactions occur between oppositely charged electrodes with separated by an ionically conductive electrolyte. For large scale storage applications, rechargeable battery materials must be inexpensive, able to cycle many times with minimal capacity fade, and have as high an energy density as possible. If a material is developed to meet these criteria, it may be able to facilitate the large scale adoptions of a variety of renewable energy technologies.

1.1 Principles of electrochemical storage

A typical battery consists of an anode, a cathode, and a separator in between the oppositely charged electrodes. The anode is typically the ion donor, and the cathode is typically the ion acceptor. However, the roles may reverse, as seen in secondary batteries, when the current flow the opposite direction and the battery charges. The separator is filled with electrolyte for ion transport between the electrodes. The electrodes must be both good ionic and electronic conductors to avoid resistive loses. In many cases, the electrode active material is not a good electronic conductor, and thus, carbon black is added to increase its electronic conductivity. A binder is also added to keep the electrode and carbon together.

Batteries are categorized into two different types: primary batteries, and secondary batteries. Primary batteries typically are only used once and the materials in the cells are irreversible transformed once discharge has occurred. Secondary batteries, or rechargeable

batteries, are able to charge and discharge reversibly over many operation cycles. Figure 2 shows a basic overview of how a secondary battery works. Although secondary batteries typically have a lower energy density per cycle when compared to primary batteries, the advantages of having a lifetime of multiple cycles outweigh this disadvantage. Overall, the total capacity of the multiple cycles in the secondary battery's lifespan is far more than the single discharge capacity output by a primary cell.

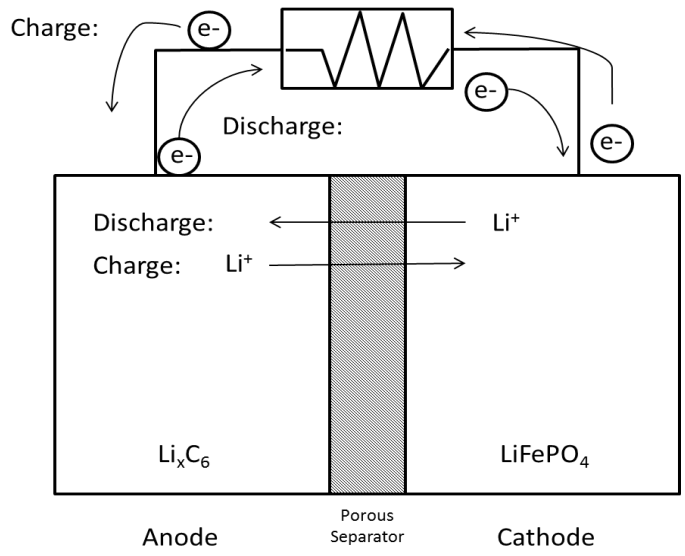

Figure 1. Basic figure portraying the process within a rechargeable battery.

1.2 Lithium ion batteries

Lithium ion batteries are currently the most extensively studied type of secondary batteries. Lithium is ideal for electrochemical work, as it is the lightest metal in the periodic table and has the greatest electrochemical potential. Its origins date back to 1912, when lithium battery was first studied under G. N. Lewis.[2] However, lithium battery research did not take off until the 1960s and 1970s, when companies saw it as an opportunity for commercialization.

During this time, companies commercialized primary lithium batteries such as lithium carbon fluoride ($Li/(CF)_n$), which was commercialized to be used in Japan during 1970.[3]

The first rechargeable lithium battery was presented by Exxon proposed a lithium-titanium(IV) sulfide system (Li/TiS_2).[4] This was first studied in a coin cell with the possibility for it to be used in watches. The next innovation comes in 1979, when Goodenough produced a lithium cobalt oxide ($LiCoO_2$) battery, which was a rechargeable battery that cycled reversibly against lithium metal at a range of 4V.[5] This discovery of lithium cobalt oxide, combined with the discovery of intercalation of lithium in graphite in 1980 leads to the production of the first prototype of a lithium ion battery in 1985, which eventually leads to the production and commercialization of lithium ion batteries by Sony in 1991.[6, 7] Another notable discovery is the discovery of manganese oxide spinel by in 1983, which paved way for research of spinel structured materials.[8] Around the same time, Sanyo produced a lithium manganese dioxide lithium battery that was used in their solar rechargeable calculators. Eventually, lithium manganese dioxide batteries would become the dominant primary battery that is used in the current market.

In 1996, Goodenough et. al. discovered lithium iron phosphate (LFP), a olivine structured material, which shows very promising results as the future of battery materials.[9] Unlike the layered lithium cobalt oxide and spinel lithium manganese oxide, LFP is very stable in structure, with the oxygen strongly bound to the structure, and is harder to heat up and explode upon short-circuiting. This stability and safety is coveted by the current market, especially the hybrid and

electric vehicle industry. Currently, research on LFP is focused on improvements in diffusion of lithium within the structure and its conductivity.

1.3 Sodium ion batteries

Although lithium ion batteries have been successful in potentially solving energy storage problems, they are limited by the availability of lithium resources and the possible raising prices this may lead to. In response to the concern of this possible problem, research has also been done with a more abundant metal: sodium. Although sodium is larger in size when compared to lithium, it is widely available at low costs, and is comparable in energy density.

Research on sodium ion battery dates back to the 1970s and 1980s. However, due to lithium ion batteries' success, research in this field has been limited. Research in sodium ion batteries only began to pick up in 2000s, when worries began to arise with the availability of lithium. Figure 2 shows the voltage and capacity at which many current sodium batteries operate at. As seen, although these sodium batteries are generally lower in capacity, they do show promising and comparable results when compared to the popular lithium manganese oxide and lithium iron phosphate materials.

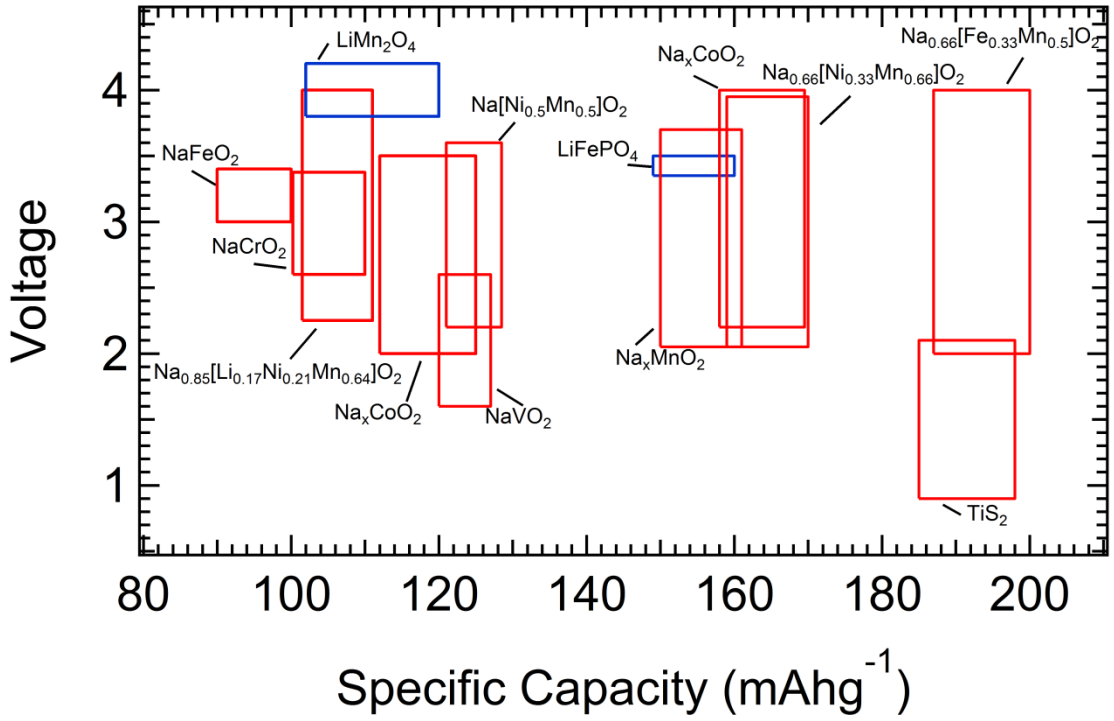

Figure 2. The general overview of the major sodium batteries. This graph also includes well known lithium batteries in blue.[34]

1.4 α-$NaFeO_2$ structure type

In order to understand the material talked about in this paper, $Na(Ni_{2/3}Sb_{1/3})O_2$, it is necessary to explore and understand its structure type.

1.4.1 α-$NaFeO_2$ structure

Many potential and current lithium ion battery materials, such as $LiCoO_2$ and $LiNiO_2$, are formed with the α-$NaFeO_2$ type structure. Generally, layered oxides are buildup of transition metals that occupy octahedral sites and forms metal oxide layers, while alkali metal ions are

arranged in between these metal oxide layers. α-$NaFeO_2$ is a rock salt related structure in which the oxygens are packed in a close-packed array. The transition metal and sodium atoms fill in a way in which they distribute orderly into the empty octahedral sites, and form general FeO_6 metal oxide layers. In between these edge sharing FeO_6 octahedral layers, NaO_6 is found in octahedral or prismatic coordination and fills in an alternating pattern of sodium and iron layers throughout the [111] direction.

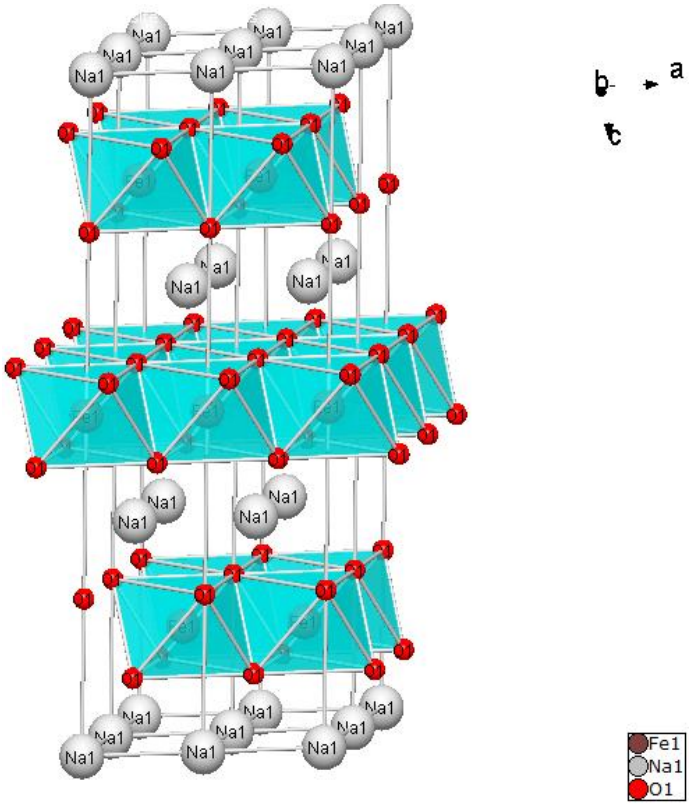

Figure 3. Crystal structure of α -$NaFeO_2$.

α-$NaFeO_2$, similar to $Na(Ni_{2/3}Sb_{1/3})O_2$ investigated in this thesis, is found crystallize in an O3 layered type structure. O3 is a categorization in the structural classification of layered oxides, as described by Delmas.[10] As described previously, typically, layered oxides form MO_6 edge

sharing octahedral layers, with alkali atoms forming between the layers in either an octahedral (O), prismatic (P), or trigonal (T) environment. This means that in an O3 type structure, alkali atoms lie in an octahedra, and shares 3 edges with three MO_6 octahedra. Usually, O3 structures follow a ABCABC stacking sequence. Similarly, a P3 type structure has its alkali atoms in a prismatic environment, sharing one face with a MO_6 octahedra, and 3 edges with three MO_6 octahedra (stacking sequence is usually ABBCCA).

1.4.2 Lithium Cobalt Oxide ($LiCoO_2$)

Lithium cobalt oxide is one of the most, if not the most, common cathode material currently used commercially.[11] While its theoretical capacity is calculated to be 248 mAh/g, only a fraction of this capacity, about 120 to 130 mAh/g, can be actually yield. This is due to its structural limitations. Studies have shown $LiCoO_2$ begins to restructure itself during charge and that $Li_{0.5}CoO_2$ has been formed in a spinel phase. [12,13] As the lithium cobalt oxide material continues to charge, its oxygen begins to distort more from its center cubic lattice, and forms a hexagonal cubic lattice by the time it fully discharges into CoO_2.[14] Due to lithium cobalt oxide's structural transformation starting at x=0.5 (for Li_xCoO_2), this is the structural limitation that has been imposed to its electrochemical results.

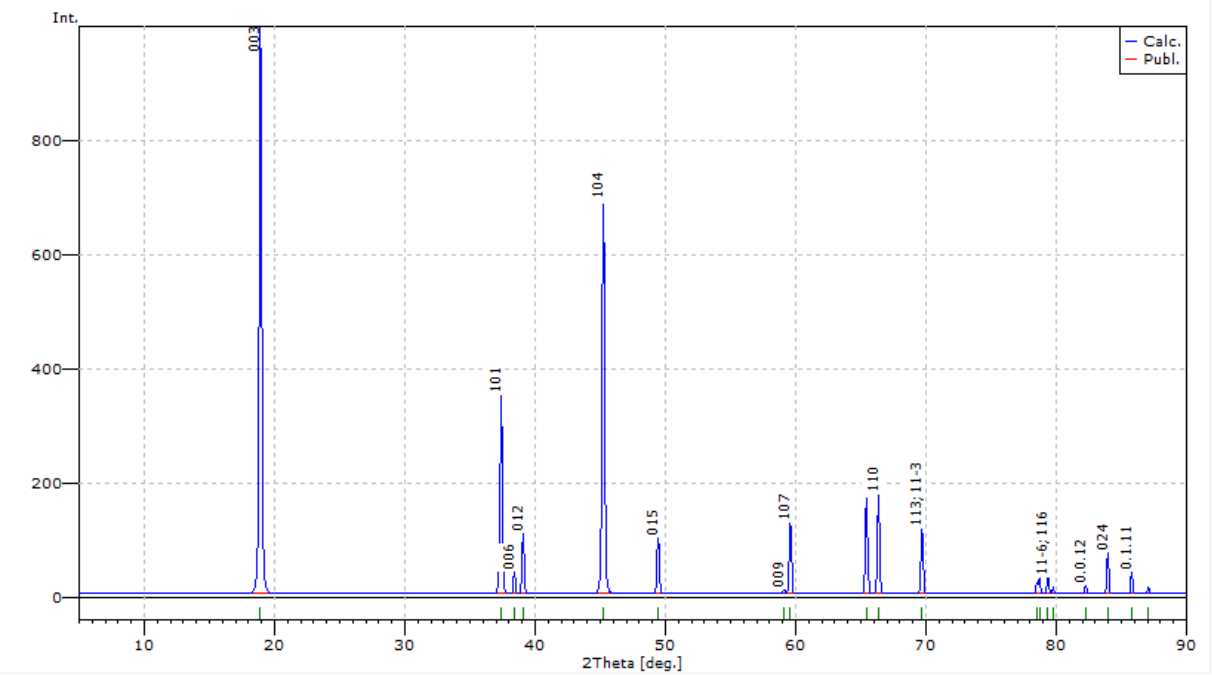

Figure 4. Calculated diffraction pattern of $LiCoO_2$ from Pearson's Crystal Data software.

Lithium cobalt oxide also faces problems with reactivity and changes in conductivity due to its structural changes during charging. While lithium cobalt oxide has been reported to be non-metallic at high lithium content, it begins to become metallic and highly conductive during charge.[15] As the material becomes more conductive during charging, it faces the risk of overcharging. This problem leads to lithium cobalt oxide facing problems of thermal stability. During overcharging, the material continues to charge even after being fully charge, and causes the decomposition of the material. This causes the production of oxygen in the cell, which may react with the anode or the electrolyte and cause an exothermic reaction to occur within the compact cell.

Other challenges lithium cobalt oxide batteries face surrounds the fact that it contains cobalt. Cobalt oxide is considered toxic and harmful to the body. Cobalt is also a rare metal, and

has a high cost. Because of this rarity and its price, cobalt is only considered for usage in smaller applications, such as watches, laptops, and cell phones.

1.4.3 Lithium Nickel Oxide ($LiNiO_2$)

Due to cobalt's rarity and price, researchers began looking for similar transition metals to replace cobalt from the $LiMO_2$ structure. Lithium nickel oxide was successfully discovered to form a similar layered structure, while other transition metal substitutes, like lithium manganese oxide, were found to form other structure types, like the spinel structure.[16,17]

Although lithium nickel oxide is found to have a layered structure, it has never been commercialized or heavily tested as a potential cathode battery material due to its structural problems. Although it is thought of as $LiNiO_2$, lithium nickel oxide has never been found in a pure state, and most reports have found it in a state with excess nickel.[18] Due to the structure having excess nickel, it is evident that nickel would be found in the lithium layer, which reduces the ability of lithium ions to flow in and out of the structure. This lower diffusion rate affects the material's performance as a battery material, and its viability as a whole as a battery material.

1.4.4 $A(M_xB_{1-x})O_2$ materials (A=Li, Na; M=Fe, Co, Ni, Cu, Zn; B=Sb, Te, Bi)

In recent years, a resurgence in the research of layered oxides have begun, with a few scientists interested in its structural properties. Researches are interested in the $A(M_xB_{1-x})O_2$ structure (A=Li, Na; M=Fe, Co, Ni, Cu, Zn; B=Sb, Te, Bi) and its magnetic properties.[19-29] Similar to the traditional layered oxides, the structure is made out of alternating ion and metal

oxide layers, with the metal layer occupied by both the smaller first row transition metals and the larger cation metals (e.g. Te, Sb, Bi). It is believed that this class of structure may be of interests as a potential battery material.

In 2007, Shirley Meng et. al., studied $Li(Ni_{2/3}Sb_{1/3})O_2$, an analog to her studies with the material $Li(Ni_{0.5}Mn_{0.5})O_2$, as a potential battery material.[30] The results that came out was not very promising. Although there was a sufficient amount of capacity (~110mAh/g) in its first cycle, the capacity quickly faded, and was less than 50mAh/g by its 5th cycle (Figure 5). It was found that after its first charge, the structure faced similar problems as lithium nickel oxide, in which the structure began to break down with the nickel metal beginning to irreversibly inhibit the lithium sites in the lithium layer. This irreversibility of nickel in the lithium layer reduces diffusion of lithium within the structure, resulting in a quick drop in capacity. The $Li_3Ni_2BiO_6$ material was also tested and had found similar results with capacity fading problems.[19]

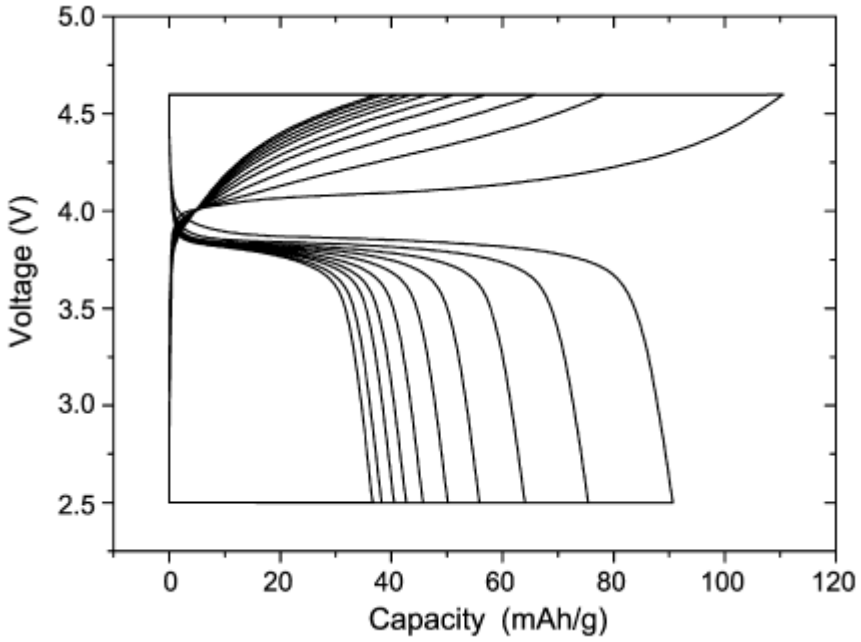

Figure 5. Electrochemical performance of $Li(Ni_{2/3}Sb_{1/3})O_2$ between 2.5 V and 4.6 V at C/20 rate. Reprinted by permission from Elsevier B.V.: X. Ma, K. Kang, G. Ceder, Y.S. Meng, J. Power Sources, 2007, 173, 550-555. Copyright 2007.

Recently, Goodenough and Tarascon have found some positive results from this $A(M_xB_{1-x})O_2$ structure.[31,32] Goodenough et. al. have been studying a $Na_2Ni_2TeO_6$ structure (space group $P6_3/mcm$) , and was successful in cycling the material without the appearance of significant capacity fading (Figure 6). The material was successful in cycling for 20 cycles between 3.0V and 4.35V with minimal capacity fading (<10mAh/g). However, this material has only been able to obtain 100mAh/g for each cycle. Tarascon et.al. showed similar results with Li_4NiTeO_6 (space group C2/m), obtaining 110mAh/g with minor capacity fading (Figure 7).

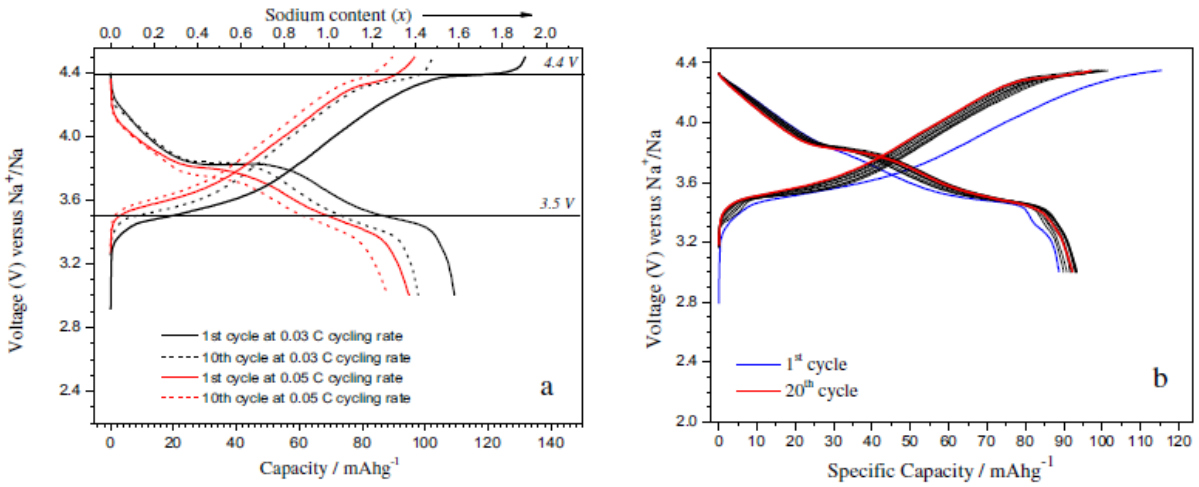

Figure 6. Electrochemical performance of $Na_2Ni_2TeO_6$ a) charge and discharge between 2.5 V and 4.5 V at 0.03 C and 0.05 C b) charge and discharge between 3.0 V and 4.35 V at 0.03 C. Reprinted by permission from Elsevier B.V.: A. Gupta, C. B. Mullins, and J.B. Goodenough, J. Power Sources, 2013, 243, 817. Copyright 2013.

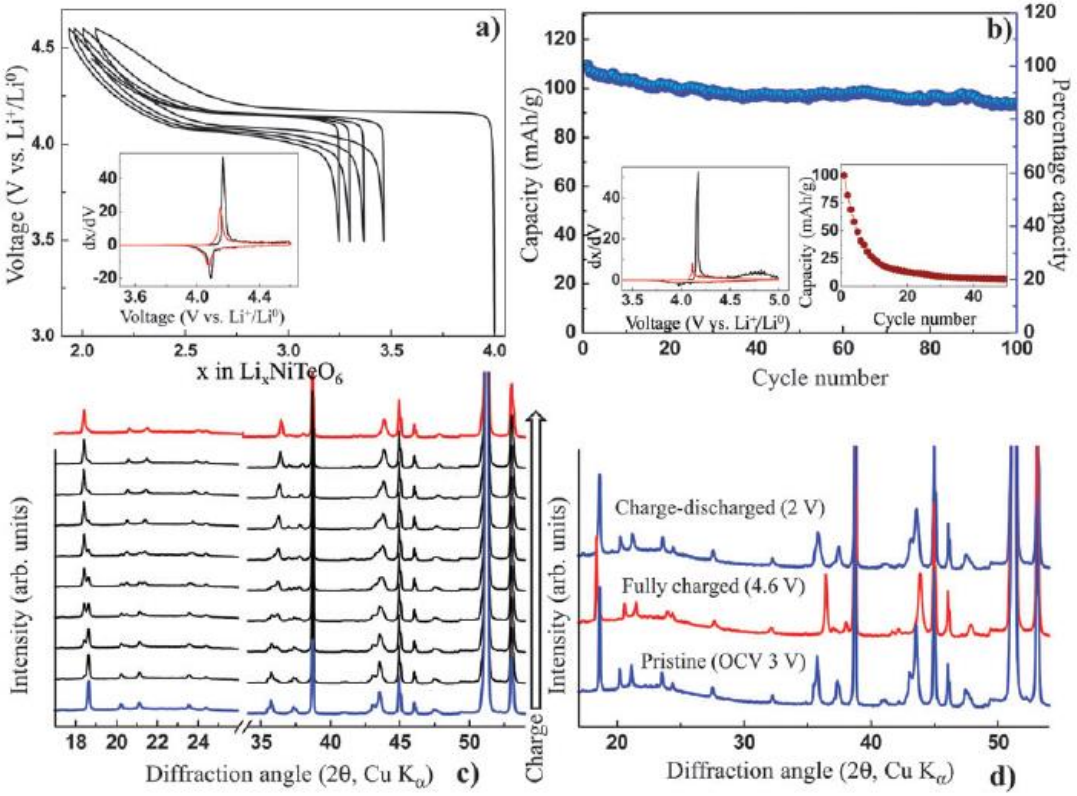

Figure 7. Electrochemical performance of Li_4NiTeO_6 a) showing voltage vs composition b) capacity vs cycle revealing the capacity retention of 100 cycles c) *In-situ x-ray study d) patterns of pristine, charged, and discharged Li_4NiTeO_6 from c).* Reprinted by permission from Royal Society of Chemistry: M. Sathiya, K. Ramesha, G. Rousse, D. Foix, D. Gonbeau, K. Guruprakash, A. S. Prakash, M. L. Doublet, and J.M. Tarascon, Chem. Commun., 2013,49, 11376-11378. Copyright 2013.

In order to achieve basic understanding of batteries, the following terms are defined:

Capacity

Capacity is the total amount of electrical charge a battery can store. Ideally, a large capacity is favorable. The following defines the theoretical capacity of a battery:

$Q = xnF$

Where Q = capacity, x = number of moles involved in the reaction, n = number of electrons involved in the reaction, and F = Faraday's constant.

or

$Q = nF/M$

Where M = molar mass of the reactant. Typically, capacity is measured in Ahg^{-1} and the second equation is used. The first equation shows us that the more of the certain electrode material is present, the higher capacity the battery has (in Ah).

Cycle life and capacity retention

The cycle life is the number of cycles a material can charge and discharge before going under a limit in capacity. Typically, the number of cycles before dropping below 80% of the first cycle capacity is the general acceptable cycle life.

Similarly, capacity retention is the amount of capacity (usually in percentage) in which a battery keeps after a certain amount of cycles. The capacity of a battery material typically decreases after

a number of charge and discharge cycles. Having high capacity retention and long cycle life is ideal and important factors to look for in when searching for a good battery material.

C-rate

C-rate is the rate relative to the material's theoretical capacity at which a constant current will be output to complete a charge or discharge. This means that 1C is the rate at which the battery will complete its charge/discharge in an hour. Similarly, 2C is the rate at which a charge/discharge is complete in half an hour, and C/2 is the rate at which charge/discharge is complete in 2 hours.

Energy density and Power density

Energy density is the energy stored in a certain volume or mass. Typically, energy density is measured in Whg^{-1} or $Wh\ cm^{-3}$. The theoretical energy density can be obtained using the equation:

$$C=q/V$$

where you substitute C for theoretical capacity and find the energy density based on the voltage. Power density is very similar in that it is the power stored in a certain mass (typically in $W\ kg^{-1}$).

Electrochemical Potential (Voltage)

Voltage is the difference in electrochemical potential within a certain boundary. For a battery, the electrode voltage (potential) can be found with the following equation:

$$E_{cell}=E_{cathode}-E_{anode}$$

Actual cell voltages are typically lower than its theoretical calculations. This may be due to polarization and the lowering of resistance within the cell due to factors such as a change in

temperature, or even time, which may cause the cell to self-discharge. The voltage of the cell at a certain state may also vary due to the current being used.

When no current is applied through the battery and the battery is at a relaxed state, the voltage at that certain state is called open circuit voltage (OCV). In contrast, when a current is applied, the voltage of the cell at that current state is called terminal voltage.

State of Charge/Depth of Discharge

The state of charge is an expression, in percentage, explaining the depth of charge capacity the system has gone through when compared to its theoretical capacity. Similarly, depth of discharge is a term expressing the how much of the theoretical capacity have the discharge gone through.

2. EXPERIMENTAL

2.1 Preparation of cathode material

2.1.1 Synthesis of disordered $Na(Ni_{2/3}Sb_{1/3})O_2$

$Na(Ni_{2/3}Sb_{1/3})O_2$ was prepared by solid state synthesis using sodium carbonate (Na_2CO_3, EMD, 99.9%), nickel hydroxide ($Ni(OH)_2$, Aldrich), and antimony oxide (Sb_2O_3, Alfa Aesar, 99.999%) . The starting materials were mixed in a stoichiometric ratio, ground thoroughly using an agate motor and pestle. A pellet was then pressed in a half inch die at 3 tons of pressure for 2 minutes using a Carver press. The pellet was then placed in an alumina crucible and heated. following a similar procedure to that reported by Zvereva *et al.*[33] The material was heated at 750˚C for 1 hour, 850˚C for 1 hour, and 1000˚C for 3 hours in air in a Barnstead Thermolyne 1300 box furnace, with intermediate grinding, pressing, and rapid cooling. The multiple heatings are necessary for removing all the carbonate and water in the sample. A bright green powder is formed.

Figure 8. A light green powder sample of disordered $Na(Ni_{2/3}Sb_{1/3})O_2$.

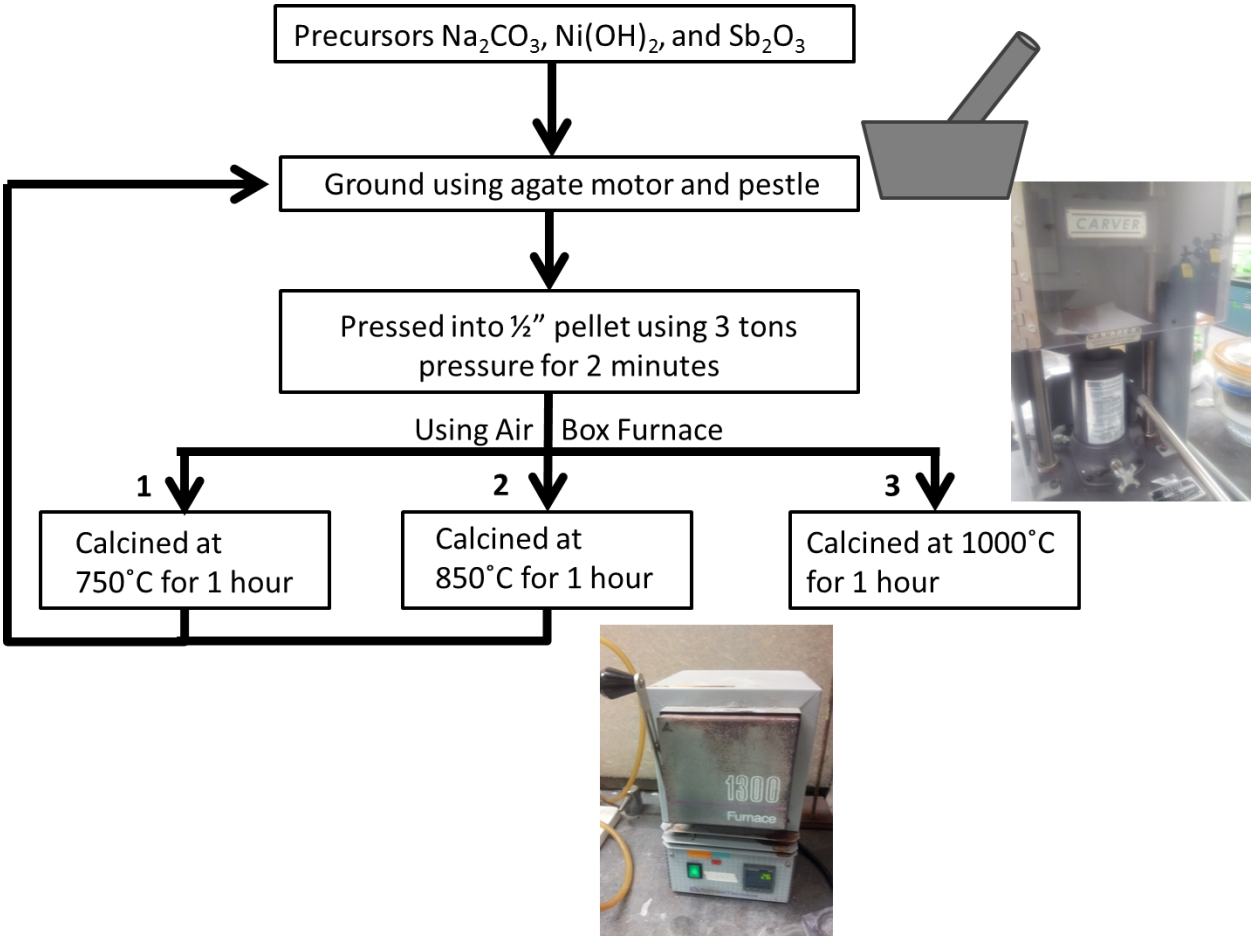

Figure 9. Synthesis process of disordered $Na(Ni_{2/3}Sb_{1/3})O_2$ including pictures of instruments used.

2.1.2 Synthesis of ordered $Na(Ni_{2/3}Sb_{1/3})O_2$

A second synthesis route was used to form a more ordered layered structure. The sample was similarly prepared, using precursors Na_2CO_3, $Ni(OH)_2$, and Sb_2O_3, but with 20% more stoichiometric Na. The starting materials were ground thoroughly, pressed into a pellet, calcined at 750˚C, and quenched to remove carbonate and moisture in the material. Similar to the disordered $Na(Ni_{2/3}Sb_{1/3})O_2$, powders were pressed into half inch diameter pellets at 3 tons pressure for 2 minutes. The sample was ground, re-pressed into pellet to minimize particle and

diffusion distance, transferred into an alumina crucible, and heated to 1200˚C for 4 hours at a heating rate of 200˚C h^{-1} in a CM Rapid Temp furnace air box furnace. The end product of this synthesis resulted in a dark green powder.

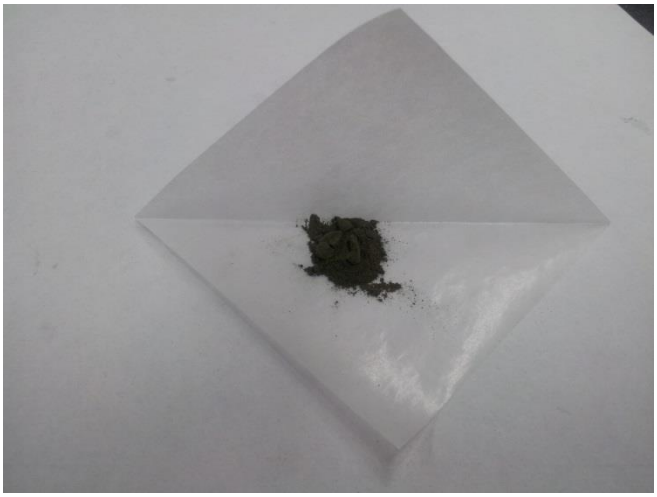

Figure 10. The olive-green ordered $Na(Ni_{2/3}Sb_{1/3})O_2$ powder.

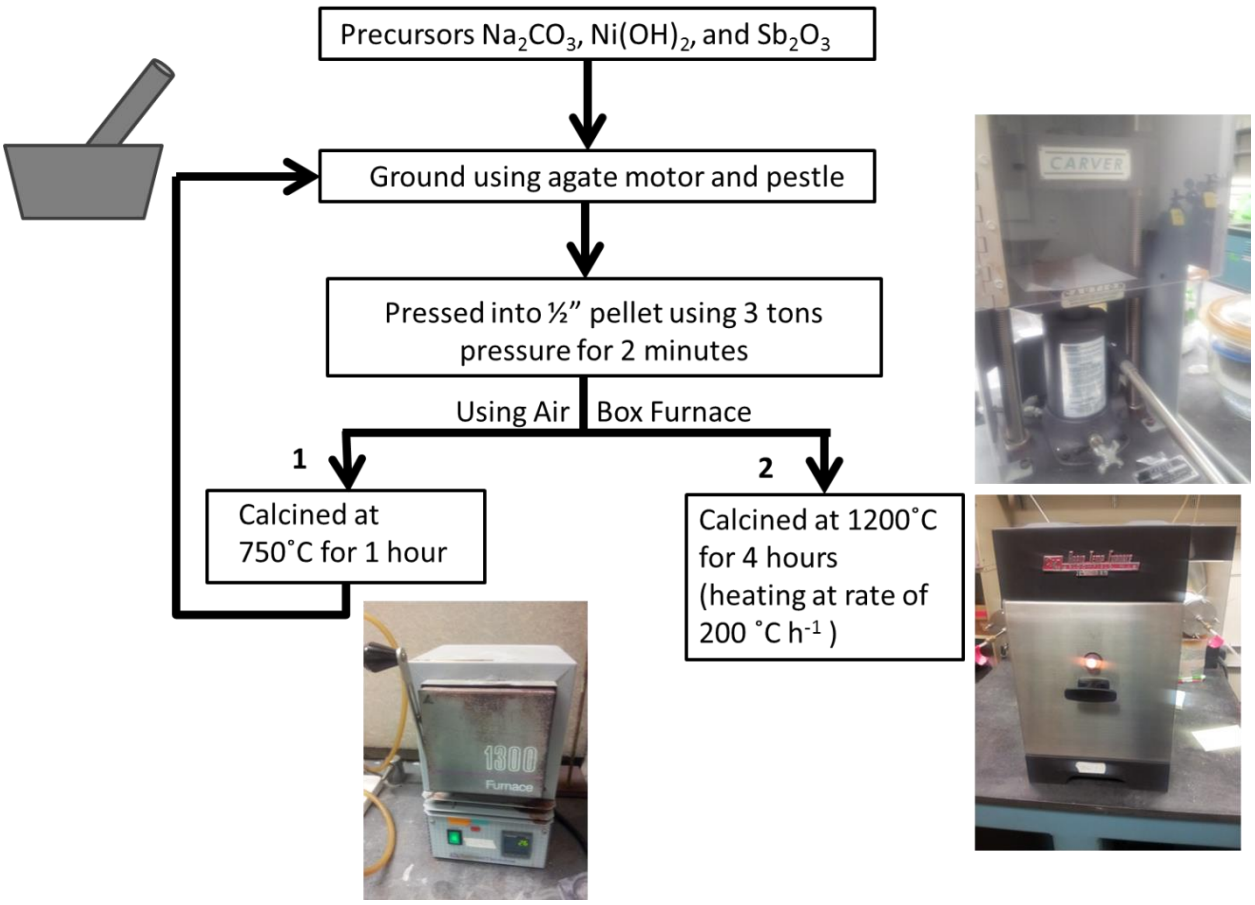

Figure 11. Synthesis process of ordered $Na(Ni_{2/3}Sb_{1/3})O_2$ including pictures of instruments used.

2.2 Preparation of electrode and cell construction for electrochemical studies

2.2.1 Preparation of composite electrode films

A thin film composite electrode was fabricated using a 70:20:10 weight ratio of the active $Na(Ni_{2/3}Sb_{1/3})O_2$ material, Super P carbon black, and polyvinylidene fluoride (PVDF) binder, respectively. The powdered material and Super P were combined and ball milled for 30 minutes in a SPEX SamplePrep8000 Mixer/Mill high-energy ball mill. After ball milling, PVDF binder was added into the carbon black and cathode material mixture and hand ground for 15 minutes using an agate motor and pestle. N-Methyl-2-pyrrolidone (NMP) was added to this mixture and mixed for about 15 minutes where it formed a slurry. The slurry was then applied onto aluminum foil and was uniformly spread using a doctor blade. The composite electrode was then placed inside an oven and dried at 100˚C overnight.

2.2.2 Assembly of battery cells

The $Na(Ni_{2/3}Sb_{1/3})O_2$ thin film electrode was used as the cathode material to assemble a button cell battery. The thin film was cut into 9/16" diameter circles and transferred into an argon atmosphere glove box. The cathode $Na(Ni_{2/3}Sb_{1/3})O_2$ material was assembled into a cell and was separated by a Whatman glass fiber separator from a piece of cut sodium metal (7/16" diameter) which acted as the anode material in the battery. The glass fiber separator was cut into 5/8" a circle and soaked with 1 M electrolyte solution of $NaPF_6$, in a solution of 1:1 (by volume) ethylene carbonate : dimethyl carbonate. The button cell batteries were allowed to rest for at least

12 hours prior to the start of measurements to ensure full contact between electrolyte and electrodes. Figure 12 shows the parts used to assemble battery cells.

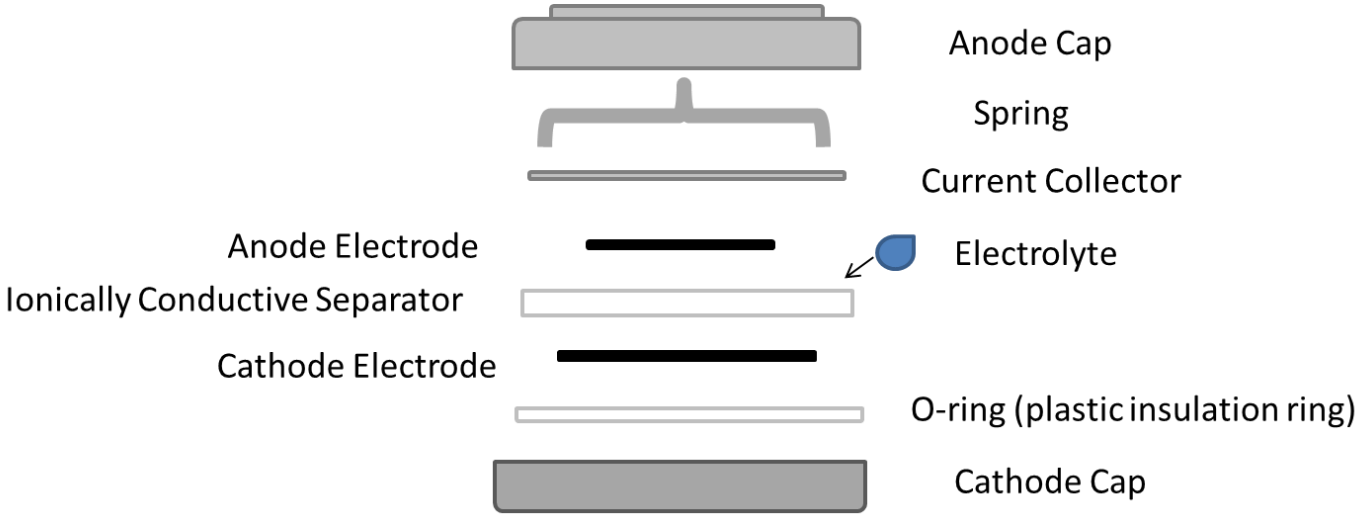

Figure 12 Basic model of a typical battery cell.

2.3 Structural characterization

Powder samples were characterized using powdered X-ray diffraction (XRD) data collected on a Bruker D8 diffractometer with Cu K_α radiation. This diffractometer has a 300 nm radius and includes a Lynx Eye detector with 192 channels. Characterization was also done using synchrotron XRD data from the 11-BM beamline of Advance Photon Source at Argonne National Laboratory. Samples were first loaded into 0.8 nm diameter Kapton capillary tubes prior, capped, and shipped. Samples were scanned at room temperature with a wavelength of 0.413686 Å. Ex-situ XRD characterizations were also done on both ordered and disordered samples. In order to study the structure of the samples at different state of charge and discharge,

battery cells of the samples were first charged and/or discharged to certain points and stopped using Arbin Instruments battery tester,. The batteries were then transferred into an argon glove box and disassembled to retrieve the cathode material samples. The cathode material was first scraped off of the aluminum foil, and then washed three times under DMC in order to wash off the binder and excess material. The sample was dried overnight and packed into Kapton capillaries for characterization by the 11-BM synchrotron XRD beamline.

2.4 Testing of the electrochemical activity

Cells were tested galvanostatically using an Arbin Instruments battery tester at room temperature. Cells were typically cycled over a voltage range of 2.5 V to 4.0 V, where the upper voltage limit was chosen due to electrochemical tests which found that charging $Na(Ni_{2/3}Sb_{1/3})O_2$ cathodes to 4.5 V leads to some irreversible high voltage (> 4.0 V) capacity during its first cycle (Fig. 13). This high voltage response is not seen during the first discharge, and is ascribed to an irreversible process that causes significant capacity fade in subsequent cycles and large polarization during the cycling. It should be noted that persistent differences in the measured charge and discharge capacities have been seen for both the ordered and $Na(Ni_{2/3}Sb_{1/3})O_2$ disordered phases. Since the capacity difference between charge and discharge decreases with increase current, this difference is ascribed to self-discharge processes associated with the presence of redox shuttling (presumably due to the dissolution of redox active Ni or Sb ions within the electrolyte). The default electrode preparation procedure was therefore modified with the addition of an extra glass fiber separator to minimize the rate of self-discharge.

Testing was also done to verify that the material was fully sodiated prior to the first charge, and that this is not the cause of the capacity difference between first charge and first discharge cycles. To test this, battery cells of both ordered and disordered $Na(Ni_{2/3}Sb_{1/3})O_2$ were cycled starting with a discharge rather than a charge sweep. It was found that both the ordered and disordered $Na(Ni_{2/3}Sb_{1/3})O_2$ cells gave no significant capacity (<1 mAh/g) in their pristine state when discharged prior to charging, indicating that either (1) all Ni is divalent in the pristine compounds and therefore not susceptible to reduction, or (2) all available Na sites are fully occupied, so that no additional Na can be inserted.

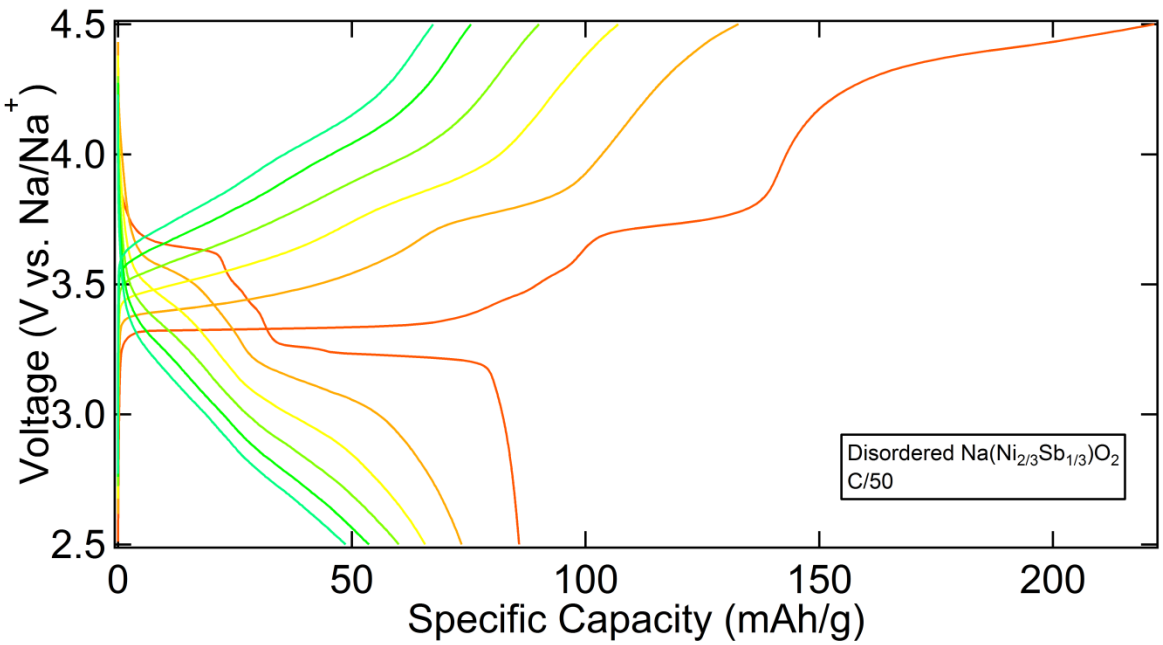

Figure 13. Disordered $Na(Ni_{2.3}Sb_{1.3})O_2$ cycled between 2.5 V and 4.5 V. Note the significant capacity fading after the first cycle.

Galvanostatic intermittent titration technique, or GITT, studies were also performed on $Na(Ni_{2/3}Sb_{1/3})O_2$. GITT was used in this experiment to study the equilibrium voltages during the deintercalation and intercalation of the material. The batteries were charged/discharged for a

certain amount of time, and then allowed to rest to study the battery at close to thermodynamic equilibrium. The disordered $Na(Ni_{2/3}Sb_{1/3})O_2$ phase were cycled at a rate of C/20 for 1 hour increments, each followed by a 30 hour rest period. Similarly, the ordered $Na(Ni_{2/3}Sb_{1/3})O_2$ phase were cycled at a rate of C/50 for 1 hour increments, each followed by a 30 hour rest period

3. RESULTS AND DISCUSSION

3.1 Structural characterization

Based on the analysis of XRD patterns, it is clear that $Na(Ni_{2/3}Sb_{1/3})O_2$ has an α-$NaFeO_2$ type layered structure at all synthesis temperatures explored in this study (900 – 1200 °C), though the reaction product has a fully ordered superstructure order at 1200 °C that is not seen at lower temperatures. The disordered $Na(Ni_{2/3}Sb_{1/3})O_2$ phase was studied using Rietveld refinement and all diffraction peaks except two can be indexed and have their intensities fit well by refinement in the simple $R\bar{3}m$ space group of α-$NaFeO_2$. The lattice parameters of disordered $Na(Ni_{2/3}Sb_{1/3})O_2$ was found to be a =3.0619(6) Å and c = 16.0549(5) Å. The small a-lattice parameter suggests that there is no specified ordering of nickel and antimony in the transition metal layer since both nickel and antimony occupy the same crystallographic site with occupancies of 0.667 and 0.333, respectively. However, the two peaks that not indexed by this subcell are indicative of a weakly developed $\sqrt{3}$ x $\sqrt{3}$ trigonal super structure, and can be indexed as the 100 and 200 reflections of this superstructure (Figure 14). This suggests that although the material is disordered on average, there is still local ordering of nickel and antimony within the octahedral layers of this layered compound. Based on prior structural studies of this phase and related phases, the Ni and Sb cations are expected to form a honeycomb lattice with each SbO_6 octahedron surrounded by six NiO_6 octahedra in an edge-sharing arrangement.

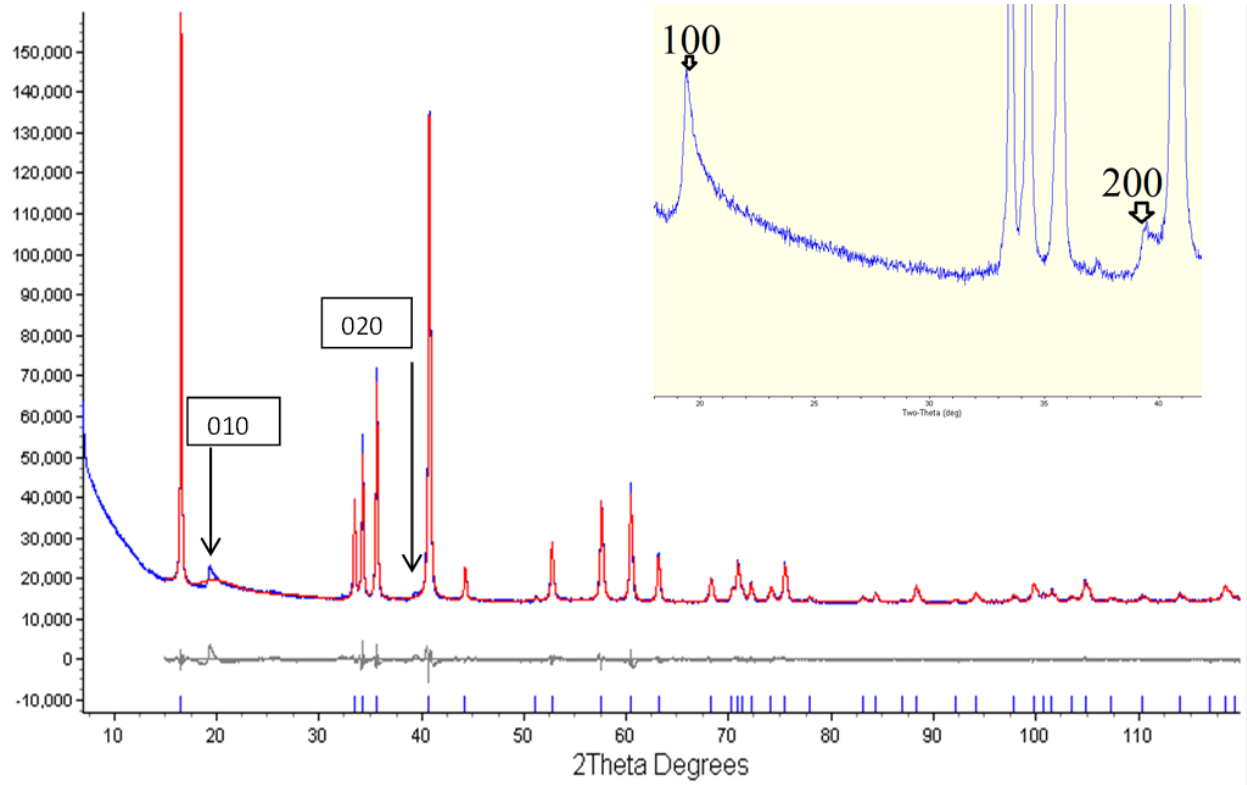

Figure 14. X-ray diffraction pattern and *R-3m* Rietveld refinement of disordered $Na(Ni_{2/3}Sb_{1/3})O_2$ synthesized at 1000˚C.

SEM was used to study the structure of the material prior to ball milling. SEM images (Figure 15) showed the presence of round, sphere like secondary particles of the disordered sample which were of sizes ranging between 10 and 20 µm. Under higher magnification, these round large particles are seen to be made up of even smaller rod-like particles that aggregated together. These rod shaped materials resemble hexagonal needles and are typically 1 to 3 µm in length and 100 to 200 nm in thickness.

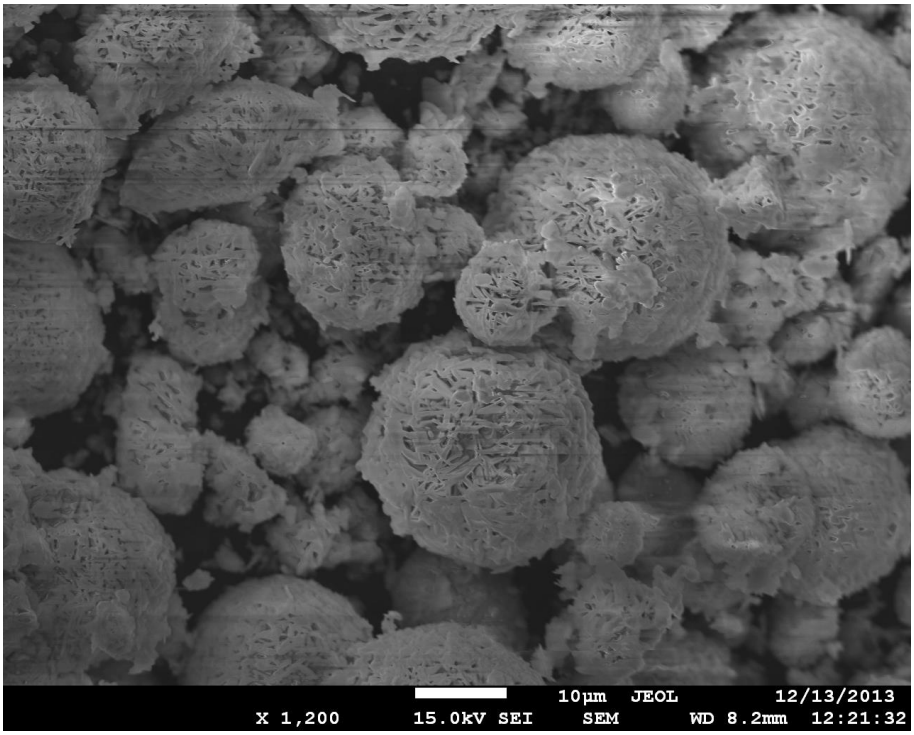

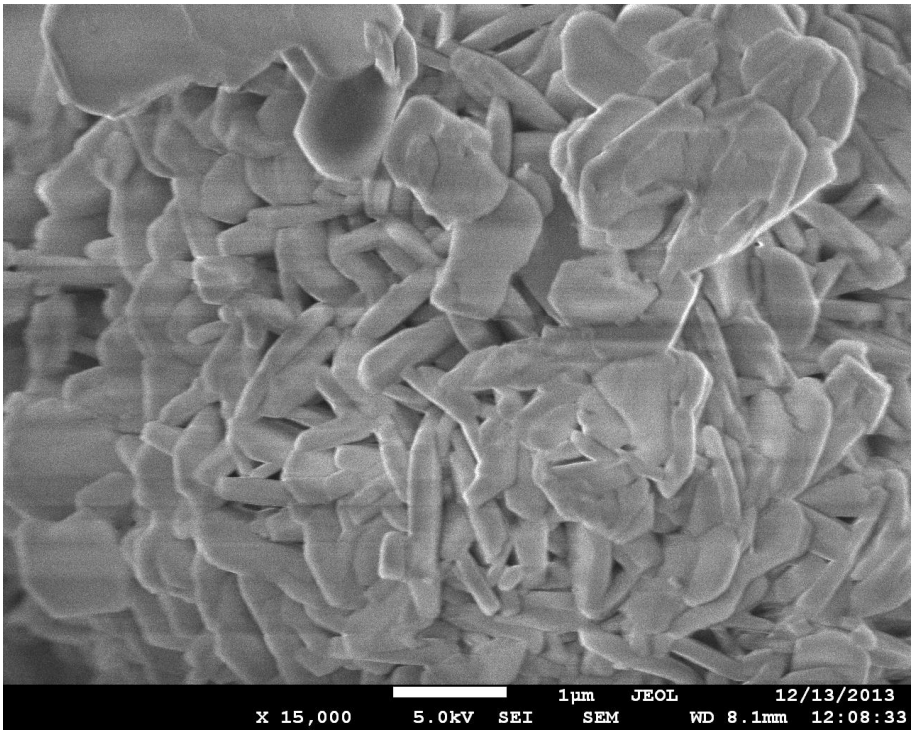

Figure 15. SEM images of disordered $Na(Ni_{2/3}Sb_{1/3})O_2$ at 1200x magnification (top) and 15000x magnification (bottom).

$Na(Ni_{2/3}Sb_{1/3})O_2$ sample synthesized at 1200˚C is found to adopt a fully ordered superstructure when 20% excess sodium is used in the reaction, though the reaction product remains disordered when only the stoichiometric amount of sodium precursors are used. The structure for the ordered sample is different than that of disordered $Na(Ni_{2/3}Sb_{1/3})O_2$, with sharp and well defined superstructure peaks clearly visible between 18˚ to 30˚ 2θ (Figure 16). This structure was successfully fit and Rietveld-refined with the lower symmetry space group C2/m with unit cell parameters of a = 5.3048(5) Å, b= 9.1847(7) Å , c= 5.6285(4) Å, and β=108.28˚. This indicates that the ordering of the nickel and antimony has good three-dimensional coherence.

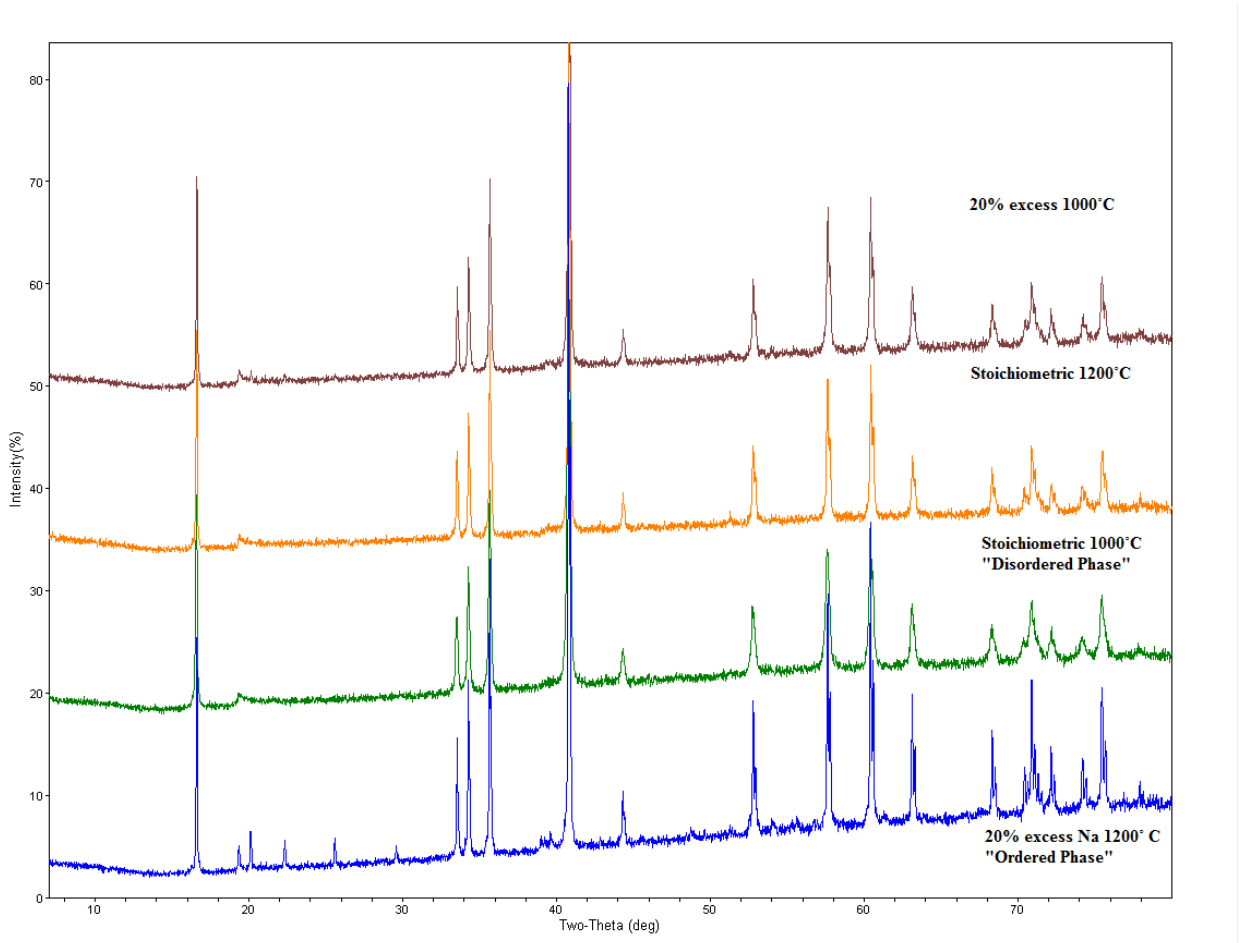

Figure 16. Comparison of XRD patterns of ordered and disordered $Na(Ni_{2/3}Sb_{1/3})O_2$. The ordered

phase has sharp superstructure peaks while the disordered phase has broad peaks superstructure which can only be seen for 00l type reflections.

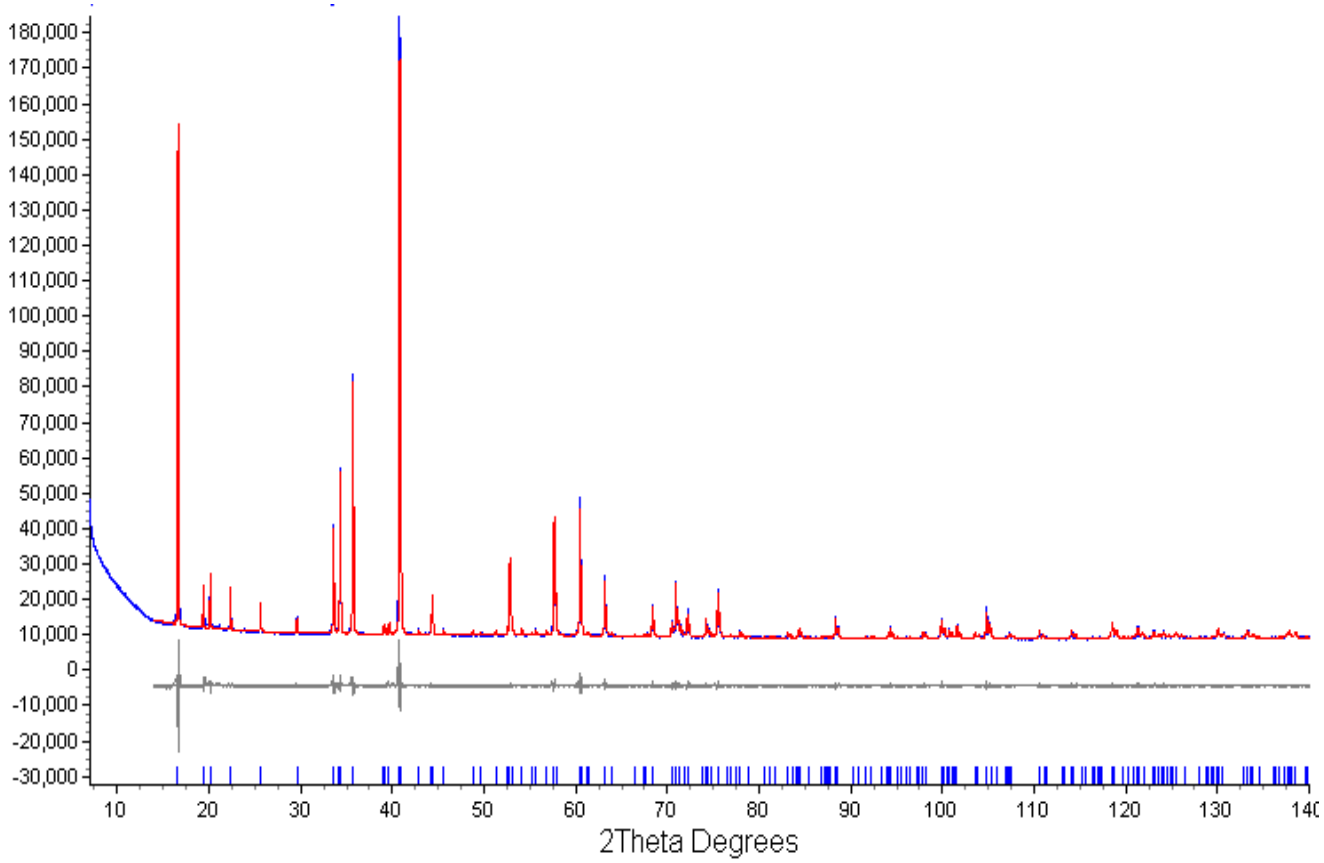

Figure 17. X-ray diffraction pattern and C2/m refinement of ordered $Na(Ni_{2/3}Sb_{1/3})O_2$ synthesized at 1200˚C.

3.2 Electrochemical characterization

The disordered $Na(Ni_{2/3}Sb_{1/3})O_2$ phase was cycled between 2.5 V and 4.0 V in 1 M $NaPF_6$ electrolyte in EC/DMC solvent. Comparative tests on hand ground and high energy ball milled powders were done to investigate the influence of particle size on performance (Figure 18). At the rate of C/50, there is a clear difference in the observed capacity. While the first charge capacity of the hand ground material is comparable to the ball milled sample, subsequent charge cycles show a significantly drop in capacity for the hand ground sample. The highest achieved discharge capacity of the hand ground sample is at most, 90 mAh/g, which is less than the 110 mAh/g capacity seen for the ball milled material. This lower capacity can be attributed to the particle size, and may be explained by the longer diffusion times in the larger particles of the hand-ground preparation.

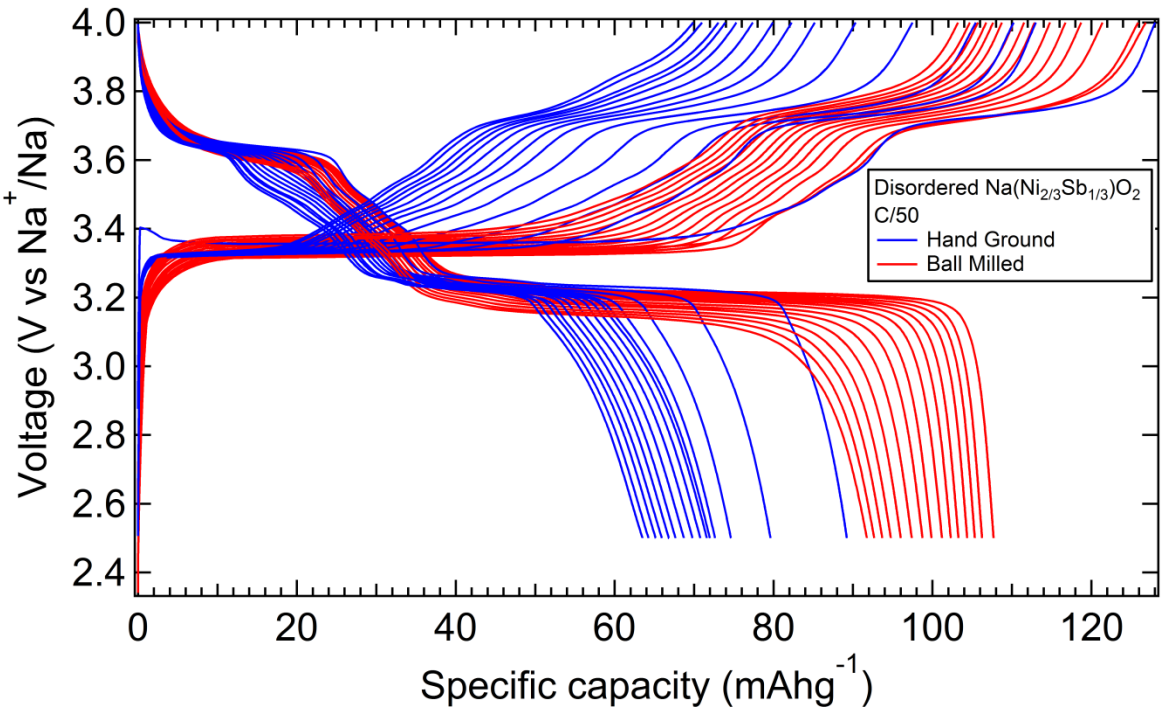

Figure 18. Comparison of hand ground and ball milled samples of disordered $Na(Ni_{2/3}Sb_{1/3})O_2$.

The electrochemical data of disordered $Na(Ni_{2/3}Sb_{1/3})O_2$ measured at a rate of C/50 shows promising results, with two plateau regions appearing throughout this 2.5 V to 4.0 V range (Figure 19). Relative to other Na-ion battery systems, these plateaus occur at very high voltages that are particularly favorable for achieving high overall energy densities. The first plateau occurs around 3.3 V, where it exhibits about 80 mAh/g capacity during this long, deep charge. Based on a theoretical capacity of 199 mAh/g associated with full Na removal, it is estimated that about 0.35 Na are removed in the first plateau. On further charging, the voltage profile next exhibits a steeply sloping region, where about 20 mAh/g capacity is accessed before reaching a second plateau. This sloping behavior is commonly observed for other layer Na-ion battery cathode materials, but this system is particularly promising in two ways. First, the sloped region makes up a small and not large fraction of the total capacity, and second, the voltage change is minimal (< 0.5 V) relative to other Na-ion systems (which might span 1 – 2 V). The higher charge plateau of disordered $Na(Ni_{2/3}Sb_{1/3})O_2$ is found around 3.7 V, and exhibits a lower capacity of only about 30 mAh/g, which equates to around 0.15 Na removed. The discharge process of disordered $Na(Ni_{2/3}Sb_{1/3})O_2$ is analogous to the charge process, though as expected, slightly lower plateau voltages (about 3.6 V and 3.2 V) are seen. The first charge capacity is about 20 mAh/g higher than that of the first discharge, indicative of either irreversible reactions with the electrolyte or of a modest amount of self-discharge occurring over the timescale of the measurement (~ 2 days for the first cycle).

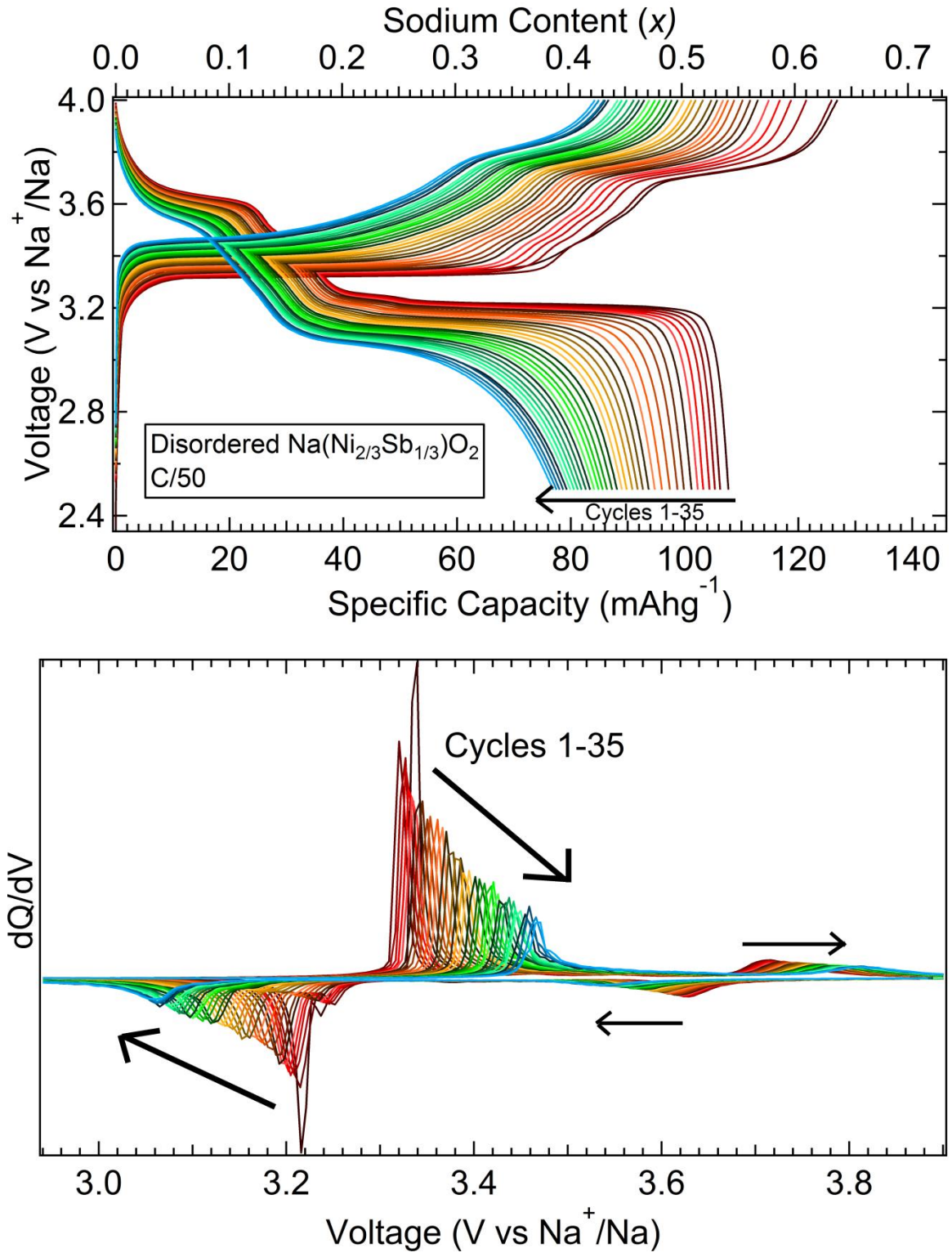

Figure 19. Electrochemical performance of disordered $Na(Ni_{2/3}Sb_{1/3})O_2$ when cycled between 2.5 V and 4.0 V at the rate of C/50 showing its capacity performance (top) and dQ/dV (bottom).

The observation of high voltage for this system is particularly encouraging. The average discharge voltage of the present system is substantially higher than that of most other Ni-containg analogues. This higher voltage may is almost certainly due to the incorporation of the Sb^{+5} into Ni-containing octahedral layers. This idea is supported by similar results from a recent paper on $Na_2Ni_2TeO_6$, where the discharge primarily occurred at an even higher voltage range (3.6 V to 4.4 V)[31]. This high voltage was ascribed to strong inductive effects caused by Te^{+6}, though we note that the elevated voltage could more simply be associated with the enhanced Coulombic repulsions between the high valence honeycomb ion (Sb^{5+} or Te^{6+}) and the oxidized state of Ni (which is typically either 3+ or 4+, though the present data do not allow us to distinguish between the two possible states).

The voltages of the main plateaus for disordered $Na(Ni_{2/3}Sb_{1/3})O_2$ do not remain constant beyond the first cycle. The polarization between charge and discharge curve increases from about 0.1 V to about 0.4 V over the first 35 cycles, with both the position and breadth of the peak in dQ/dV data varying across cycles (Figure 19). Another change that occurs as the battery is cycled is that the difference between charge and discharge capacity eventually disappears over time (Figure 20), as the total capacity of disordered $Na(Ni_{2/3}Sb_{1/3})O_2$ decreases through successive cycles. Only samples cycled at low rates are effective at retaining their capacity, with a modest loss of about 20% in capacity over the first 30 cycles. Samples cycled at C/10 or faster are found to lose 80% of their capacity over the same number of cycles. The poor rate performance of this material is highlighted in Figure 21, which compares the first cycle data of the disordered $Na(Ni_{2/3}Sb_{1/3})O_2$ material operated at different C-rates. Higher C-rates result in a very large difference in voltage between the charge and discharge plateaus in the hysteresis. This

could be associated with slow kinetics for the structural transition that occurs during the two-phase region.

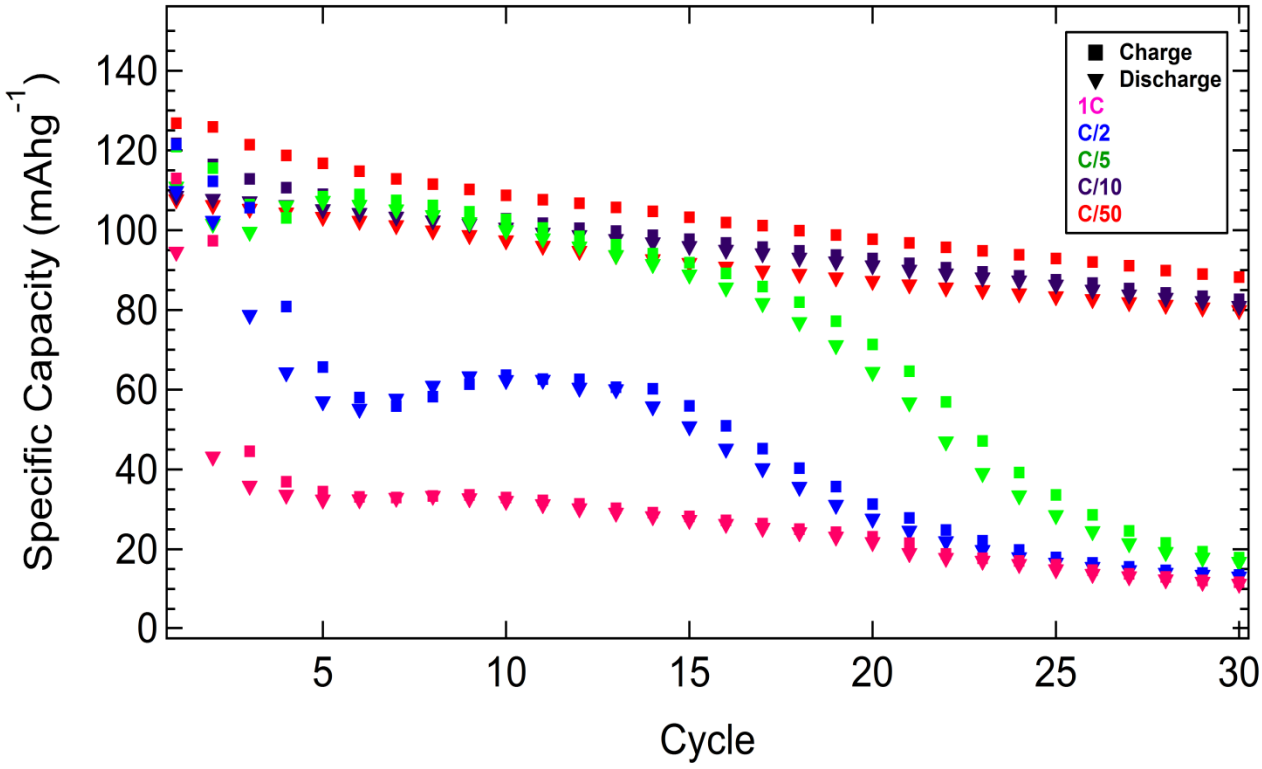

Figure 20. Capacity retention of the disordered $Na(Ni_{2/3}Sb_{1/3})O_2$ cell cycled at different C-rates.

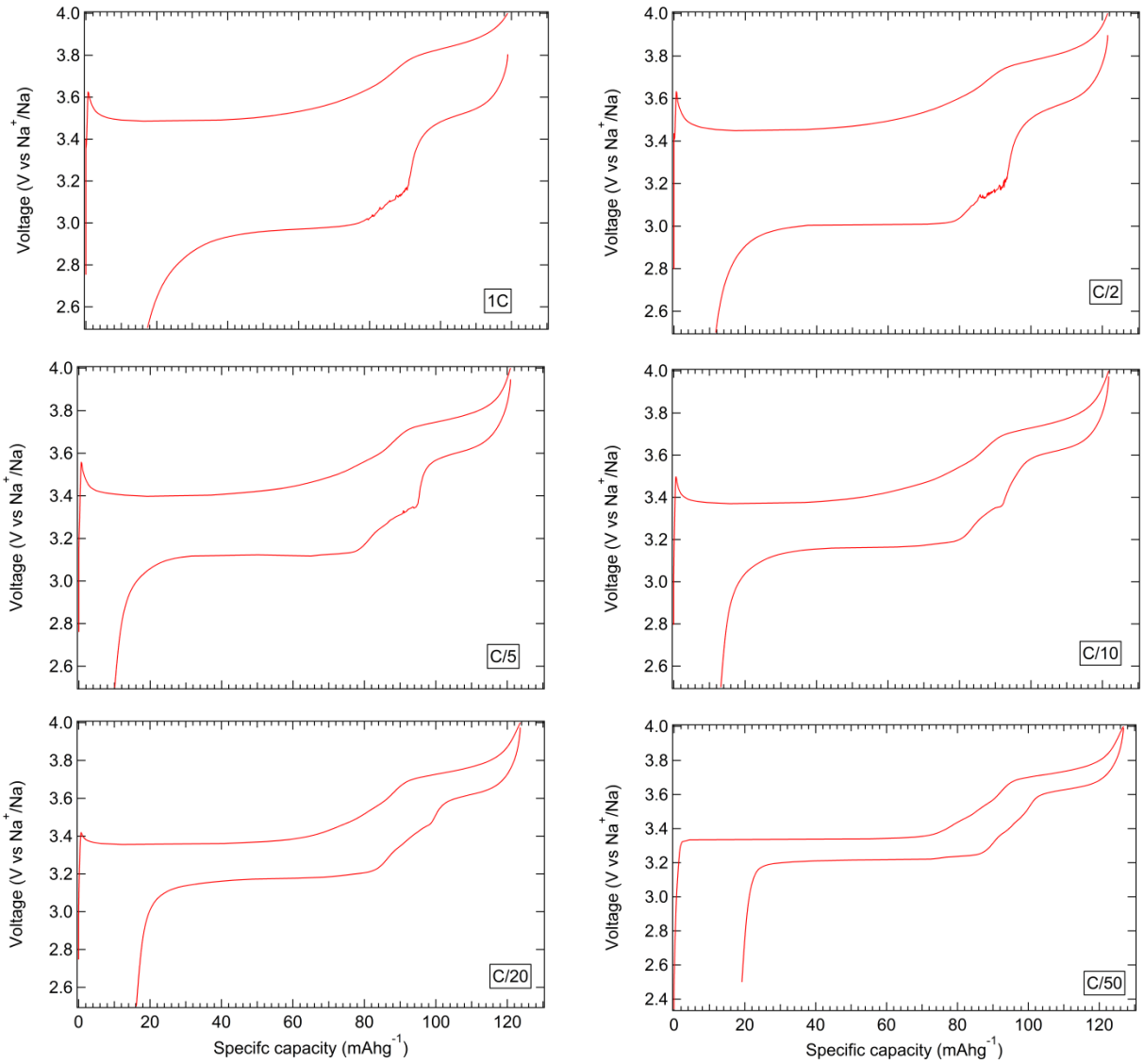

Figure 21. The first cycle, including charge and discharge, of disordered $Na(Ni_{2/3}Sb_{1/3})O_2$ at different C-rates.

In order to test the first redox feature in this system independently (as it may potentially have better reversibility than subsequent processes), electrochemical tests were done on the disordered $Na(Ni_{2/3}Sb_{1.3})O_2$ material with a the upper cutoff voltage reduced to 3.4 V from the original 4.0 V (Figure 22). The first charge capacity of the first plateau resulted was 78 mAh/g and the first discharge capacity was 67 mAh/g, which were not much changed relative to the

cycling over the full electrochemical window used previously. The lower lower cutoff voltage does reduced the capacity fade somewhat, but the loss in capacity is still substantial (about 11% over 30 cycles) and shows no sign of abating in subsequent cycles.

.

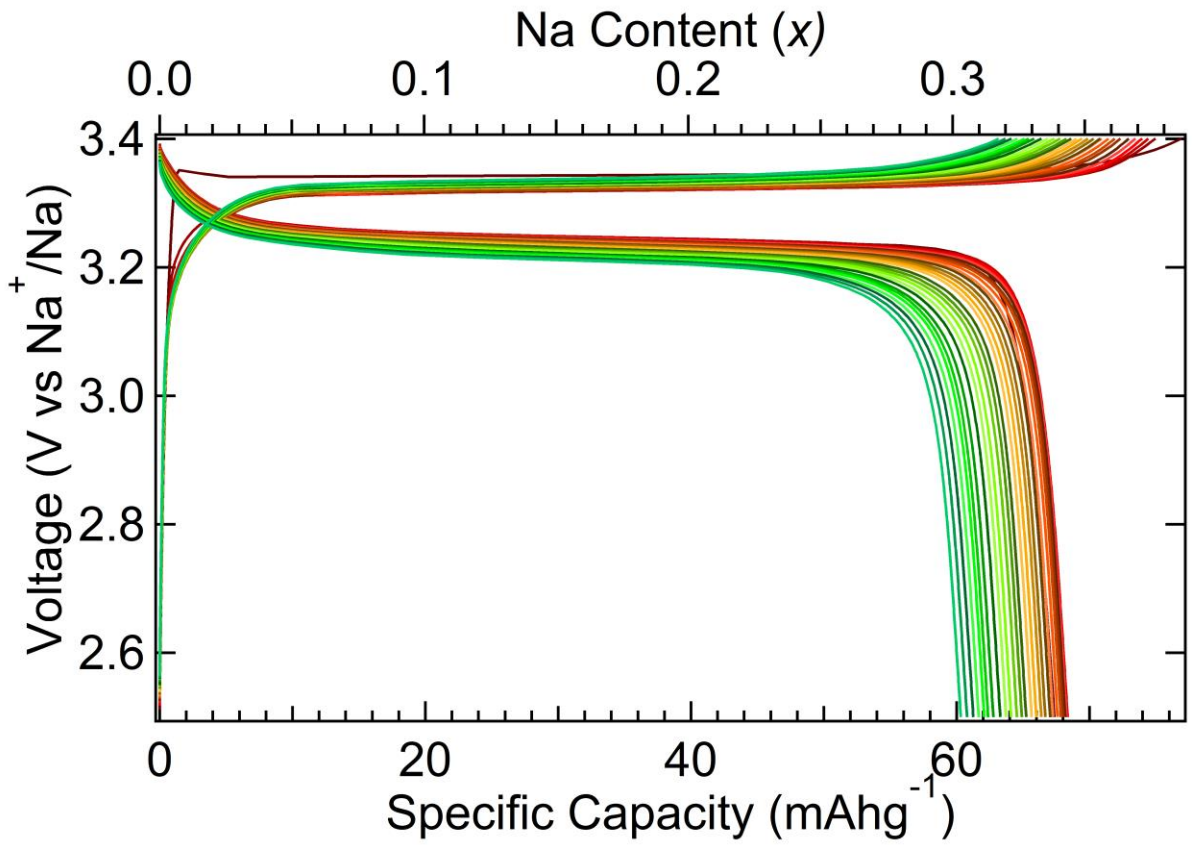

Figure 22. Electrochemical performance of disordered $Na(Ni_{2/3}Sb_{1/3})O_2$ cycled with a lower cutoff voltage, from 2.5 V to 3.4 V, at a rate of C/50.

The ordered $Na(Ni_{2/3}Sb_{1/3})O_2$ phase exhibited clear structural differences from the disordered phase, and was electrochemical tested under similar conditions (2.5 V to 4.0 V; 1 M $NaPF_6$ electrolyte in EC/DMC) to see if it exhibited enhanced electrochemical performance. The ordered $Na(Ni_{2/3}Sb_{1/3})O_2$ phase showed general electrochemical features that were very similar to

that of the disordered phase, with two prominent plateaus observed (Figure 23). However, the plateaus present in the ordered phase are flatter and more extended than those of the disordered phase. At a rate of C/50, the ordered phase delivers a discharge capacity of about 133 mAh/g (0.65 Na per formula unit) which shows about a 25 mAh/g improvement over the disordered phase. Of this capacity, about 90 mAh/g capacity (0.45 Na) comes from the first plateau present at around 3.3 V. The voltage then goes through a sloped region, with about 20 mAh/g of capacity before it reaches the next plateau. For the second plateau, located at about 3.7 V, about 35 mAh/g capacity is delivered, which equates to about 0.18 Na. The discharge profile mirrors the charge profile, but with plateaus at slightly lower voltages (at around 3.6 V and 3.2 V).

The first discharge capacity is about 10 mAh/g lower than that of the first charge cycle (Fig. 24). The difference between the capacity of charge and discharge disappears in later cycles, with the capacity difference between charge and discharge on the second cycle being only about 6 mAh/g (4.4% difference). The capacity fading at a C/50 rate is minimal, with only a loss of 9% capacity (12 mAh/g) in 25 cycles. The ordered phase shows the same type of voltage phase as the disordered phase, though the in polarization increases less quickly. While the ordered phase has the advantages of improved capacity and reduced voltage fade, it has worse rate performance than the disordered phase and quickly loses capacity even at slow rates of C/20. The worse rate performance of the ordered phase could be due to larger particle sizes associated with the higher synthesis temperature, or could alternatively indicate a lower density of nucleation centers for the two-phase reaction mechanism that is implied by the voltage plateaus.

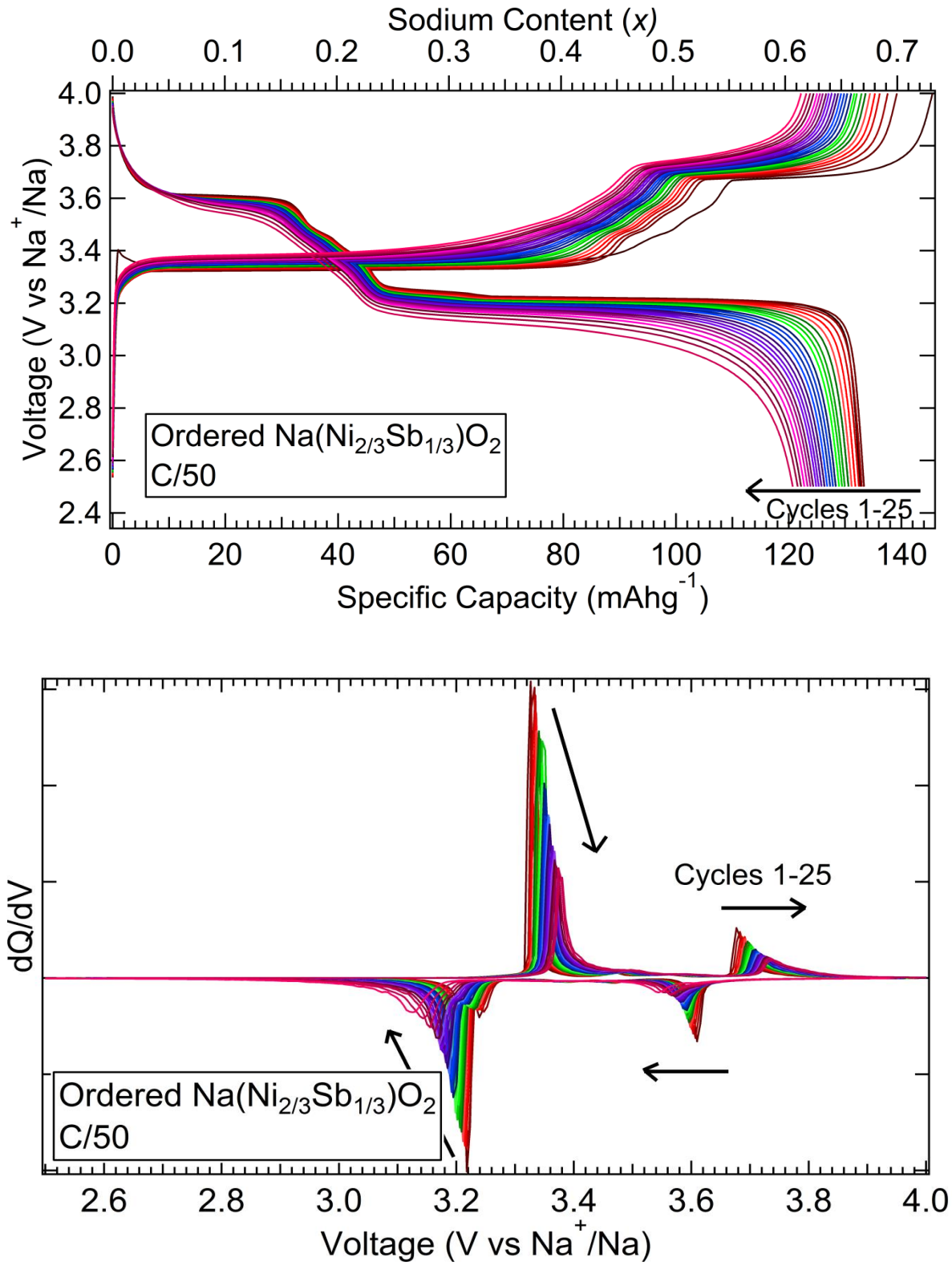

Figure 23. Electrochemical performance of ordered $Na(Ni_{2/3}Sb_{1/3})O_2$ when cycled between 2.5 V and 4.0 V at the rate of C/50 showing its capacity performance (top) and dQ/dV (bottom).

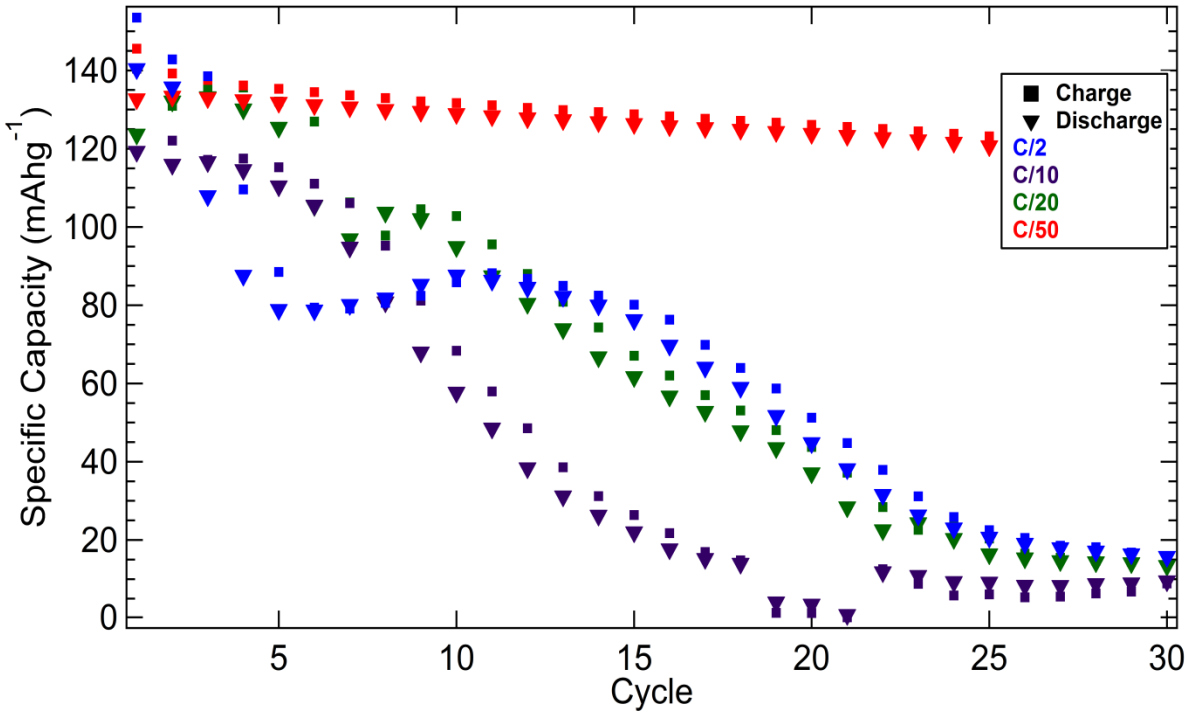

Figure 24. Capacity retention of the ordered $Na(Ni_{2/3}Sb_{1/3})O_2$ cell cycled at different C-rates.

The reversibility of the low voltage plateau of ordered $Na(Ni_{2/3}Sb_{1/3})O_2$ was tested with a using a reduced cutoff voltage of 3.4 V (Figure 25) to investigate the capacity retention associated with this redox process. The first discharge delivers about 100 mAh/g of capacity, suggesting that up to 0.5 Na per formula unit can be cycled at this voltage. The capacity fade over 30 cycles is still about 10%, and is not substantially improved relative to tests over the full electrochemical window of this phase. The difference between the charge and discharge capacity is less than 10 mAh/g beyond the first cycle.

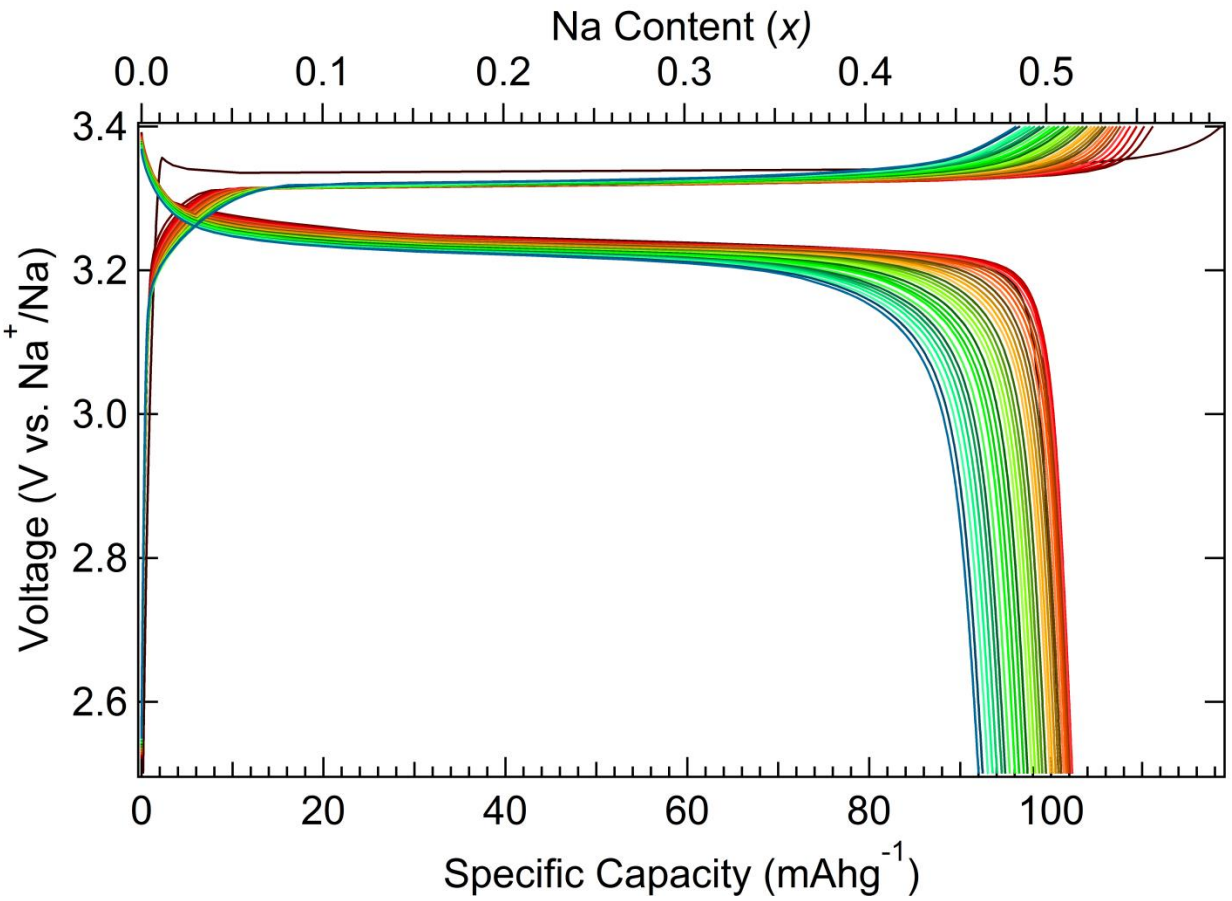

Figure 25: Electrochemical performance of ordered $Na(Ni_{2/3}Sb_{1/3})O_2$ cycled with a lower cutoff voltage, from 2.5 V to 3.4 V, at a rate of C/50.

3.3 Ex-situ x-ray diffraction

Ex- situ studies were done on $Na(Ni_{2/3}Sb_{1/3})O_2$ to study structural changes that occur during electrochemical cycling. Both disordered and ordered $Na(Ni_{2/3}Sb_{1/3})O_2$ were studied at a few different states of charge (CH) or discharge (DIS) to explore the progression of phases during cycling. The most obvious change in the XRD patterns at the different states of charge is the increase in *c*-axis length that occurs as Na is removed (Figure 26). During charging, the original disordered $R\bar{3}m$ $Na(Ni_{2/3}Sb_{1/3})O_2$ peaks weaken in intensity, while the peaks for the expanded second phase strengthen in intensity. At the end of charge, there are no diffraction peaks from the pristine phase indicating that the structure has fully converted. The desodidated $Na(Ni_{2/3}Sb_{1/3})O_2$ structure was indexed and refined to have a similar rhombohedral lattice, but with a R3m space group and the atom positions characteristic of a P3 stacking sequence (trigonal prismatic Na sites between octahedral layers) rather than the O3 stacking of the pristine phase (octahedral Na sites between layers). During the discharge (sodiation) process, the structural changes are reversed. As the material is discharged, a 2-phase mixture first forms, followed by the regeneration of the original $Na(Ni_{2/3}Sb_{1/3})O_2$ phase. The electrochemical response of disordered $Na(Ni_{2/3}Sb_{1/3})O_2$ exhibits two major plateaus (each of which should reflect a different 2-phase transition) as well as at least two additional electrochemical features between 3.3 and 3.6 V. Based on the available data, it appears that the O3/P3 transition is associated with the first major plateaus at 3.3 V, and that a more complete set of *in situ* diffraction data is required will be required to elucidate the subtle structural transitions associated with the remaining electrochemical features. These are hinted at in the two different positions of the first 00L peak (~4.25° 2θ) in the P3 phase of ordered $Na(Ni_{2/3}Sb_{1/3})O_2$ at voltages between 3.25 and 3.65 V (Figure 27).

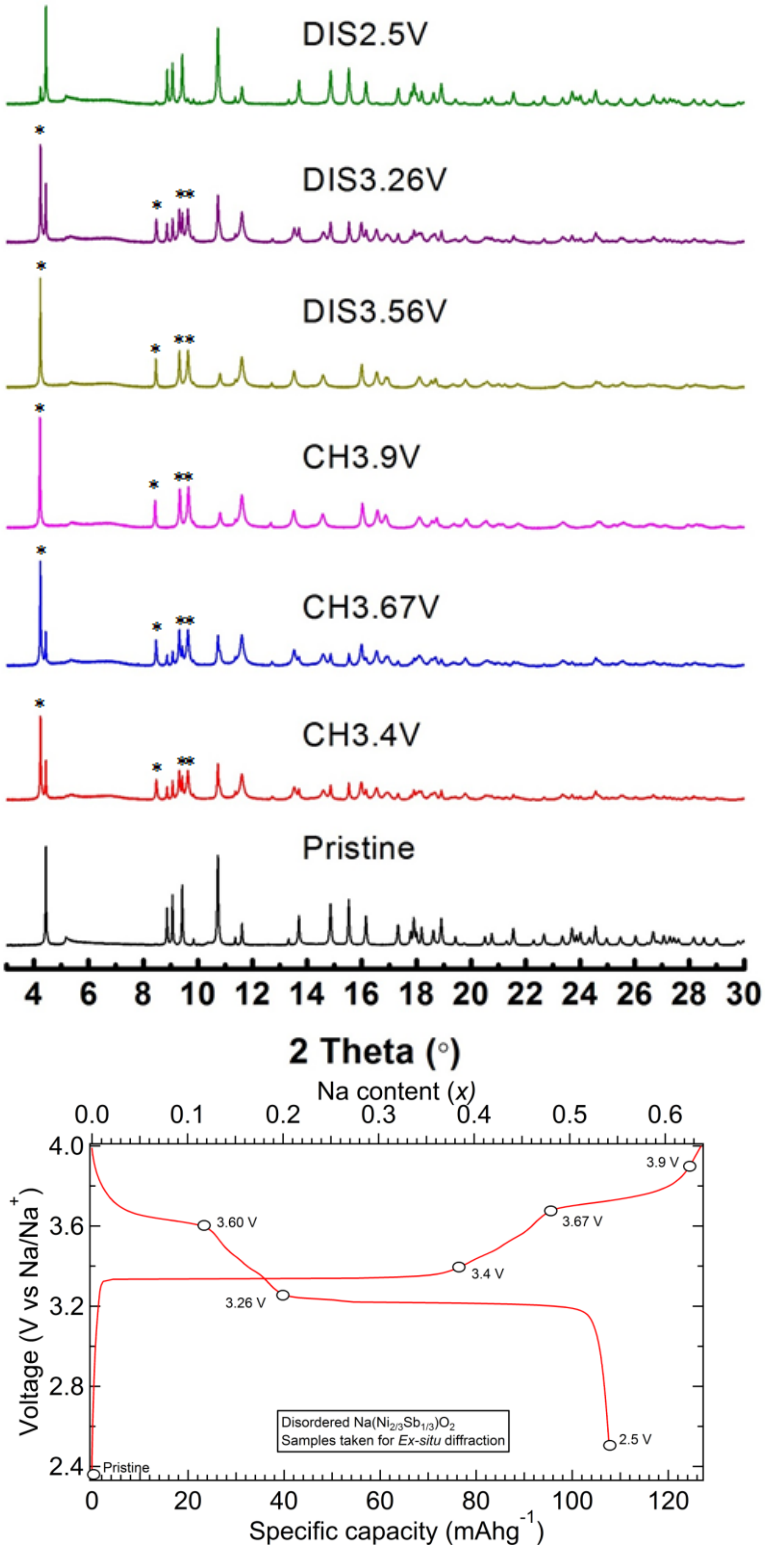

Figure 26. *Ex-situ* studies of disordered $Na(Ni_{2/3}Sb_{1/3})O_2$ showing the X-ray diffraction patterns at different states of charge (top), as well as the electrochemical response of a typical cell (bottom), where * marks peaks from desodiated R3m phase.

Ex-situ studies were done on the ordered phase in order to better understand the transformation pathway for ordered $Na(Ni_{2/3}Sb_{1/3})O_2$ structure during cycling. During charging, the intensities of the original ordered $Na(Ni_{2/3}Sb_{1/3})O_2$ phase begin to weaken until it disappears at the end of the desodiation, which is similarly seen in the *ex-situ* studies of the disordered $Na(Ni_{2/3}Sb_{1/3})O_2$. However, the cycling of the disordered $Na(Ni_{2/3}Sb_{1/3})O_2$ produced only one two-phase reaction that converted the original material to a desodiated phase. This differs from the *ex-situ* results of ordered phase that presents two different phases throughout the desodiation process (Figure 27). At 3.4 V, the end of the first electrochemical plateau during charging, the appearance of a second phase appears, while the original phase weakens in intensity. The second phase, however, begins to disappear by the beginning of the second plateau, at 3.65V, and the formation of a third phase, with a larger volume, appears. This third phase continues in its formation and is found to be the only phase present at the end of charge. This process is then able to be successfully reversed during sodiation, where discharging of the material leads to the appearance of the second phase, before returning to the formation of the original ordered $Na(Ni_{2/3}Sb_{1/3})O_2$. This *ex-situ* study ultimately shows the presence of two 2-phase reactions, one occurring at each plateau, which forms two new and different phases in the process.

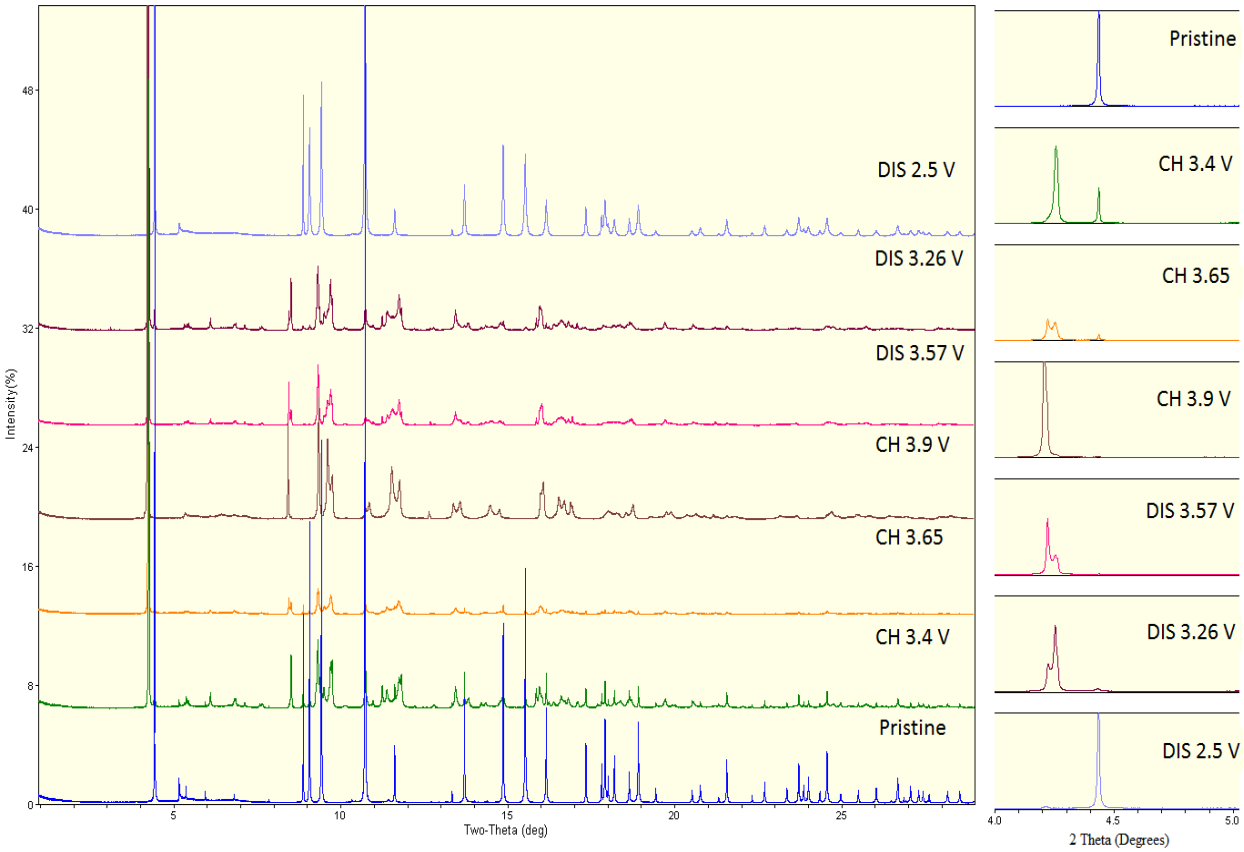

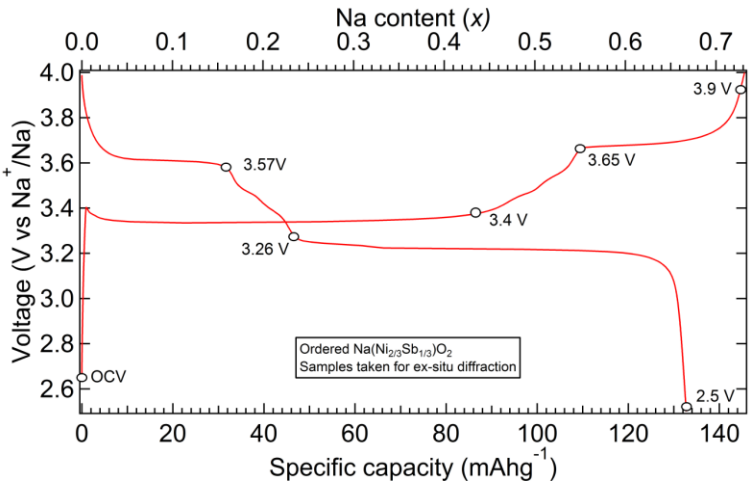

Figure 277. *Ex-situ* studies of ordered $Na(Ni_{2/3}Sb_{1/3})O_2$ showing the x-ray diffraction patterns at different states of cycling (top) and at which points these different states were stopped during the electrochemical cycling (bottom). Note that top left shows the diffraction patterns in the range of 0˚ to 30˚ 2θ, while the top right shows the range of 4˚ to 5˚ 2θ.

3.4 GITT analysis

GITT is an electrochemical technique for identifying the voltage at near thermodynamic equilibrium conditions, using long relaxation times that usually allow equilibrium conditions to be attained. With this data, it is often possible to identify whether the plateaus that are present represent two-phase regions or solid solution regions that are only slightly sloped. Figure 28 shows the GITT data for the disordered $Na(Ni_{2/3}Sb_{1/3})O_2$ phase, cycled at a rate of C/20 for 1 hour increments, each followed by a 30 hour rest period. A close examination of the data suggests that full relaxation was achieved at each measurement step. Two possible plateaus are seen in original electrochemical cycling data (C/50 rate, Figure 19). The low voltage plateau has a characteristic voltage of 3.27 V with no more than a 30 mV difference from this voltage seen after relaxation. The voltage in the region of this plateau relaxes by about 100 mV during the resting period of the cell, but curiously, jumps by about 300 mV when the current is applied again. This suggests that about 200 mV of overpotential are needed to initiate the O3 → P3 structural transition, a conclusion which is supported by the relatively rapid relaxation (182 seconds) of this initial overpotential. Furthermore, the need for an initial overpotential behavior is not seen for the corresponding P3 → O3 transition on discharge, which indicates easier that this transition is more facile or that a high concentration of the defects necessary to initiate the structural transition may already be present in the sample.

The higher voltage plateau is not sampled as well in the present electrochemical data, so it is difficult to draw conclusions about the nature of the structural transition associated with this redox feature centered near 3.67 V. There are a total of four relaxed voltages which are within

50 mV of this estimated thermodynamic potential. Furthermore, the large difference (50 mAh/g) between the current sourced during charge and discharge suggests that self-discharge may be substantially influencing the data and that the correspondence between current and state of charge is somewhat approximate. Throughout the first charge/discharge cycle, the only data point which required relaxation of more than 150 mV was the last point of the charge cycle, suggesting that the C/50 data is generally quite close to the intrinsic behavior of this phase.

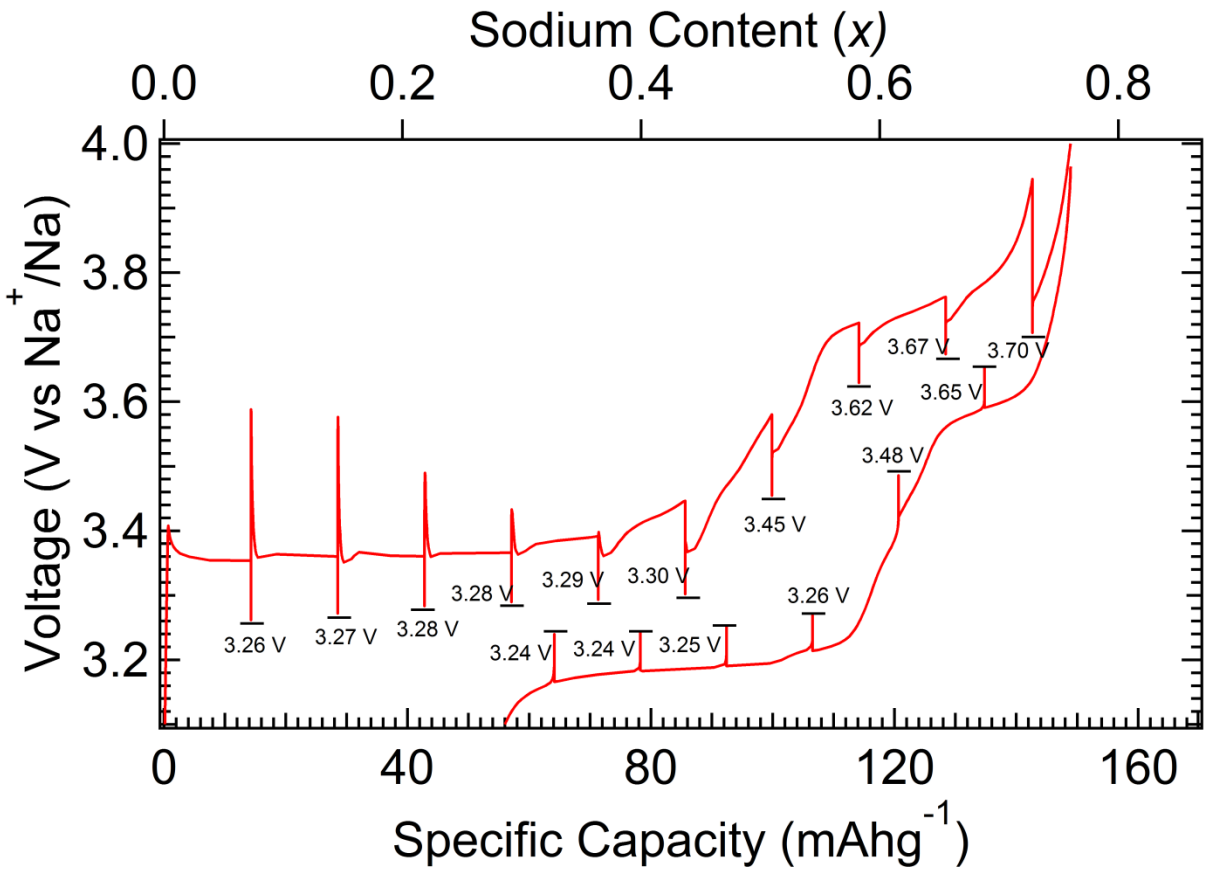

Figure 28. GITT of disordered $Na(Ni_{2/3}Sb_{1/3})O_2$ at a rate of C/20 cycled from 2.5 V to 4.0 V.

The corresponding GITT study of the ordered phase is shown in Figure 28. The first plateau again shows a well-defined first plateau. In contrast to the disordered phase, no evidence

for the requirement of a large overpotential for driving the O3→ P3 transition is seen for any point other than at the initiation of charging. The lower voltage plateau is again always observed within 30 mV of 3.27 V, while the high voltage plateau relaxes to a slightly lower average voltage of 3.64 V with 5 data points within 20 mV of this central voltage. There is again a substantial difference between the current sourced on charge (170 mAh/g) and discharge (130 mAh/g), consistent with some self-discharge occurring over the timescale of this experiment (~1 month).

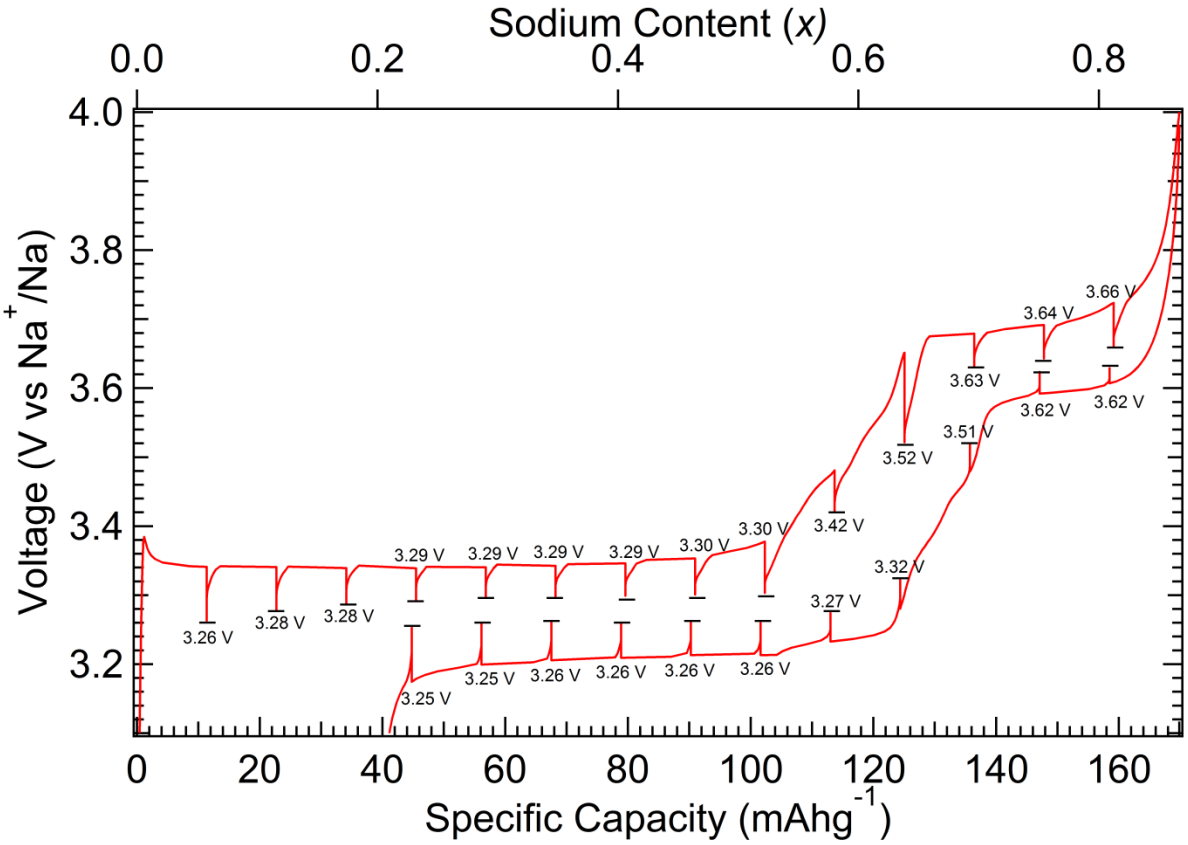

Figure 29. GITT of ordered $Na(Ni_{2/3}Sb_{1/3})O_2$ at a rate of C/50 cycled from 2.5 V to 4.0 V.

4. CONCLUSION

Ordered and disordered (synthesized at 1000˚C and 1200˚C, respectively) forms of $Na(Ni_{2/3}Sb_{1/3})O_2$ were prepared and characterized. $Na(Ni_{2/3}Sb_{1/3})O_2$ belongs to the α-$NaFeO_2$ structure type with the average structure best described by the space group of $R\bar{3}m$. Disordered $Na(Ni_{2/3}Sb_{1/3})O_2$ has a unit cell of a = 3.0619(6) Å and c = 16.0549(5) Å, while ordered $Na(Ni_{2/3}Sb_{1/3})O_2$ has a unit cell of a= 5.3048(5) Å, b= 9.1847(7) Å , c= 5.6285(4) Å, and β=108.28˚ that is best described by the monoclinic space group *C2/m*. Both disordered and ordered phases exhibit a honeycomb ordering of nickel and antimony in the metal layer, but the latter has three dimensional and not just two-dimensional ordering. The electrochemical response of both phases is qualitatively similar and is dominated by a low voltage (3.27 V) and high voltage plateaus (3.65 V), with a small amount of capacity in what appears to be a strongly sloping solid solution regime between the two plateaus. The ordered $Na(Ni_{2/3}Sb_{1/3})O_2$ phase has a higher discharge capacity (133 mAh/g *vs.* 108 mAh/g) and less capacity fade than the disordered phase. However, disordered $Na(Ni_{2/3}Sb_{1/3})O_2$ exhibits better rate performance than ordered $Na(Ni_{2/3}Sb_{1/3})O_2$. GITT studies suggest that this improvement is not due to improved nucleation (which in fact appears easier in the ordered phase), and the improvement is therefore ascribed to the reduced particle size of that results from the lower temperature synthesis of the disordered phase. It is therefore expected that particle size reduction is a viable approach to substantially improve the rate performance of this system, as well as potentially improving the total accessible capacity. Ex-situ XRD studies on $Na(Ni_{2/3}Sb_{1/3})O_2$ show a transformation from an initial O3 layered phase to a P3 layered phase during the low voltage plateau, with the P3 stacking sequence persisting as further Na ions are removed. This structural transformation is reversed on discharge. The XRD data on the ordered $Na(Ni_{2/3}Sb_{1/3})O_2$ shows the presence of the

same O3 and P3 phases, and also provides evidence for a secondary modification of the P3 phase. The experimentally achieved energy density of $Na(Ni_{2/3}Sb_{1/3})O_2$ is quite promising (~130 mAh/g at discharge voltages of 3.1 V and higher), and it is expected that the performance of this phase can be further improved through chemical substitution.

REFERENCES

[1] U.S. Energy Information Administration, *Monthly Energy Review April 2014*, Table 1.3
[2] Lewis, G. N. *J Am Chem Soc*, **1913**, 35, 1448.
[3] Watanabe, N.; Fukuba, M. *U.S. Patent* 3,536,532, **1970**.
[4] Whittingham, M. S. *Science* **1976**, *192*, 1126.
[5] Mitzushima, K.; Jones, P. C.; Wiseman, P. J.; Goodenough, J.B. *Mater. Res. Bull.* **1980**, *15*, 783.
[6] Yazami, R.; Touzain, P. *J. Power Sources*, **1983**, 9, 365.
[7] Akira, Y.; Kenichi, S.; Takayuki, N. *U.S. Patent* 4668595, **1985**.
[8] Thackeray, M. M.; David, W. I. F.; Bruce, P. G.; Goodenough, J. B. *Mater. Res. Bull.* **1983**,18 , 461.
[9] Padhi, A.K.; Nanjundaswamy, K.S.; Goodenough, J.B. Electrochem. Soc. Meeting Abstracts, **1996**, 96-1, 73.
[10] Delmas, D.;Fouassier, C.; Hagenmuller, P. *Physica*, **1980**, 99B, 81-85.
[11] Ozawa, K. *Solid State Ionics* **1994**, *69*, 212.
[12] Rossen, E.; Reimers, J. N.; Dahn, J. R. *Solid State Ionics* **1993**, *62*, 53.
[13] Gabrisch, H.; Yazimi, R.; Fultz, B. *J. Electrochem. Soc.* **2004**, *151*, A891.
[14] Amatucci, G. G.; Tarascon, J. M.; Klein, L. C. *J. Electrochem. Soc.* **1996**, *143*, 1114.
[15] Imanishi, N.; Fujiyoshi, M.; Takeda, Y.; Yamamoto, O.; Tabuchi, M. *Solid State Ionics* **1999**, *118*, 121.
[16] Thackeray, M. M. *Prog. Solid State Chem* **1997**, *25*, 1.
[17] Yonemura, M.; Yamada, A.; Kobayashi, H.; Tabuchi, M.; Kamiyama, T.; Kawamoto, Y.; Kanno, R. *J. Mater. Chem.* **2004**, *14*, 1948.
[18] Dahn, J. R.; Sacken, U. v.; Michal, C. A. *Solid State Ionics* **1990**, *44*, 87.
[19] Berthelot, R.; Schmidt, W.; Muir, S.; Eilertsen, J.; Etienne, L.; Sleight, A.W.; Subramanian, M.A.; *Inorg. Chem.*, **2012**, 51 ,5377–5385
[20] Schmidt, W.; Berthelot, R.; Etienne, L.; Wattiaux, A.; Subramanian, M.A. *Mater. Res. Bull.* **2014**, 60, 292-296.
[21] Schmidt W.; Berthelot, R.; Sleight, A.W.; Subramanian, M.A. *Solid State Chem.*, **2013**, 201, 178-185.
[22] Zvereva, E.A.; Evstigneeva, M.A.; Nalbandyan, V.B.; Savelieva, O.A.; Ibragimov, S.A.; Volkova, O.S.; Medvedeva, L.I.; Vasiliev, A.N.; Klingeler, R.; Buechner, B. *Dalton Trans.* **2012**,41, 572-580.
[23] Nalbandyan, V.B.; Avdeev, M.; Evstigneeva, M.A. *Solid State Chem.***2013**, 199, 62-65.
[24] Kumar, V.; Gupta, A.; Uma, S. ***Dalton Trans.*, 2013**,42, 14992-14998
[25] Seibel, E.M.; Roudebush, J.H.; Wu, H.; Huang, Q.; Ali, M.N.; Ji, H.; Cava, R.J. *Inorg. Chem.*, **2013**, 52, 13605–13611
[26] Evstigneeva, M.A.; Nalbandyan, V.B.; Petrenko, A.A.; Medvedev, B.S.; Kataev, A.A. *Chem. Mater.*, **2011**, 23, 1174–1181
[27] Viciu, L.; Huang, Q.; Morosan, E.; Zandbergen, H.W.; Greenbaum, N.I.; McQueen, T.; Cava, R.J. *Solid State Chem.* **2007**, 180, 1060-1067.
[28] Politaev, V.V.; Nalbandyan, V.B.; Petrenko, A.A.; Shukaev, I.L.; Volotchaev, V.A.; Medvedev, B.S. *Solid State Chem.* **2010**, 183, 684-691.
[29] Nalbandyan, V.B.; Politaev, V.V. *Solid State Sci.***2009**, 11, 144-150.
[30] Ma, X.; Kang, K.; Ceder, G.; Meng, Y.S. *J. Power Sources.* **2007**,173, 550-555

[31] Gupta, A.; Mullins, C.B.; Goodenough, J.B. *J. Power Sources.* **2013**, 243, 817-821.
[32] Sathiya, M.; Ramesha, K.; Rousse, G.; Foix, D.; Gonbeau, D.; Guruprakash, K.; Prakash, A.S.; Doublet, M.L.; Tarascon, J.M. *Chem. Commun.*, **2013**,49, 11376-11378.
[33] Zvereva, E.A.; Savelieva, O.A.; Titov, Y.D.; Evstigneeva, M.A.; Nalbandyan, V.B.; Kao, C.N.; Lin, J.Y.; Presniakov, I.A.; Sobolev, A.V.; Ibragimov, S.A.; Abdel-Hafiez, M.; Krupskaya, Y.; Jahne, C.; Tan, G.; Klingeler, R.; Buchner, B.; Vasiliev, A.N. *Dalton Trans.*, **2013**,42, 1550-1566.
[34] Yabuuchi, N.; Kajiyama, M.; Iwatate, J.; Nishikawa, H.; Hitomi, S.; Okuyama, R.; Usui, R.; Yamada, Y.; Komaba, S. *Nat. Mater.*, **2012**, 11, 512-517.